Steiner, T., Meka, S. R., Rheingans, B., Bischoff, E., Waldenmaier, T., Yeli, G., Martin, T. L., Bagot, P. A. J., Moody, M. P., & Mittemeijer, E. J. (2016). Continuous and discontinuous precipitation in Fe-1 at.%Cr-1 at.%Mo alloy upon nitriding; crystal structure and composition of ternary nitrides. *Philosophical Magazine*, *96*(15), 1509-1537. https://doi.org/10.1080/14786435.2016.1167282

Continuous and discontinuous precipitation in Fe-1 at.%Cr-1 at.%Mo alloy upon nitriding; crystal structure and composition of ternary nitrides

Tobias Steiner[1,2], Sai Ramudu Meka[1], Bastian Rheingans[3], Ewald Bischoff[1], Thomas Waldenmaier[2], Guma Yeli[4], Tomas L. Martin[4], Paul A.J. Bagot[4], Michael P. Moody[4], Eric J. Mittemeijer[1,3]

[1]*Max Planck Institute for Intelligent Systems (formerly MPI for Metals Research), Heisenbergstrasse 3, 70569 Stuttgart, Germany*

[2]*Robert Bosch GmbH Heat Treatment Processes and Heat Treatment Technology (CR/APM4), Postbox 300240, 70442 Stuttgart, Germany*

[3]*Institute for Materials Science, University of Stuttgart, Heisenbergstrasse 3, 70569 Stuttgart, Germany*

[4]*Department of Materials, University of Oxford, Parks Road, Oxford OX1 3PH, United Kingdom*

Abstract:

The internal nitriding response of a ternary Fe-1 at.%Cr-1 at.%Mo alloy, which serves as a model alloy for many CrMo-based steels, was investigated. The nitrides developing upon nitriding were characterized by X-Ray diffraction, Scanning Electron Microscopy, Electron Probe Microanalysis, Transmission Electron Microscopy, and Atom Probe Tomography. The developed nitrides were shown to be (metastable) ternary mixed nitrides, which exhibit complex morphological, compositional, and structural transformations as a function of nitriding time. Analogous to nitrided binary Fe-Cr and Fe-Mo alloys, in ternary Fe-Cr-Mo alloys initially continuous precipitation of fine, coherent, cubic, NaCl-type nitride platelets, here with the composition $(Cr_{½},Mo_{½})N_{¾}$, occurs, with the broad faces of the platelets parallel to the $\{100\}_{\alpha\text{-Fe}}$ lattice planes. These nitrides undergo a discontinuous precipitation reaction upon prolonged nitriding leading to the development of lamellae of a novel, hexagonal

$CrMoN_2$ nitride along $\{110\}_{\alpha\text{-Fe}}$ lattice planes, and of spherical cubic, NaCl-type $(Cr,Mo)N_x$ nitride particles within the ferrite lamellae. The observed structural and compositional changes of the ternary nitrides have been attributed to the thermodynamic and kinetic constraints for the internal precipitation of (misfitting) nitrides in the ferrite matrix.

Keywords: nitriding, Fe-Cr-Mo, microstructure characterization, $CrMoN_2$, atom probe tomography (APT)

1. Introduction

Many technologically important steels are based on the Fe-Cr-Mo(-C) system, due to superior hardenability, toughness, anti-corrosion properties, and microstructural stability at elevated temperatures, associated with the combined presence of Cr, Mo and C in these steels [1]–[3]. Further enhancement of the fatigue, wear and corrosion resistance of these steels can be achieved by nitriding, a thermochemical surface treatment process by which N is introduced into the surface adjacent regions of the steel components [4]–[6]. Cr is present in most nitriding steels due to its strong interaction with N leading to the formation of Cr-N-nitrides. Mo is usually added to nitriding steels to enhance the properties of the unnitrided core of the components. However, Mo does also interact with N, albeit relatively slowly [7]. Hence, in order to optimize the nitriding response of the material to achieve desired property profiles, control and, to that end, understanding of the interaction of inwardly diffusing N with both alloying elements present in steel is necessary. This is the background for the present investigation of the nitriding behavior of Fe-1 at.%Cr-1 at.%Mo alloy.

Upon nitriding of binary Fe-Cr [8]–[13] and Fe-Mo [7], [14] alloys initially cubic, NaCl-type CrN and cubic, NaCl-type γ-Mo_2N (here 50 % of the octahedral-interstitial sublattice are not occupied by N), respectively, form as (semi-)coherent platelets with their broad faces parallel to the $\{100\}_{\alpha\text{-Fe}}$ lattice planes and with a Baker-Nutting (BN) orientation relationship (OR) [15] with the ferrite matrix. The kinetics of formation of CrN is considerably faster than that of γ-Mo_2N. This initial microstructure, composed of coherent nitrides finely dispersed in the ferrite matrix, is commonly referred to as *continuously precipitated (CP)*. Upon nitriding for prolonged time, Fe-Cr alloys with sufficiently high Cr-content undergo a

discontinuous coarsening (DC) reaction [8]–[13], whereas in Fe-Mo alloys a *discontinuous precipitation (DP)* reaction of γ-Mo_2N to δ_3-MoN occurs [7].

Information on the nitriding behavior of Fe-Cr-Mo-based technical alloys is scarce [16]–[18] and fundamental investigation on the nitriding behavior of ternary Fe-Cr-Mo alloys has not been carried out until now. The interaction of both Cr and Mo in a ternary Fe-Cr-Mo model alloy with the N introduced by a nitriding treatment is the focal point of the current work on the gaseous nitriding of a model Fe-1 at.%Cr-1 at.%Mo alloy (henceforth abbreviated as Fe-1Cr-1Mo). Some preliminary results of this project have been presented at a recent conference [19]. The here presented detailed characterization of the developing nitrides, employing X-ray diffraction (XRD), scanning electron microscopy (SEM), electron probe microanalysis (EPMA), transmission electron microscopy (TEM), and Atom Probe Tomography (APT), reveals the sequential development of ternary nitrides.

2. Experimental

2.1. Specimen Preparation and Nitriding

The Fe-1Cr-1Mo alloy was prepared by melting elemental Fe (99.98 wt.%), Cr (99.99 wt.%), and Mo (99.95 wt.%) in an induction furnace under a protective Ar atmosphere, followed by casting into a Cu crucible. The surfaces of the cast were ground with SiC paper to remove surface contaminants. The cast slab was cold rolled to a sheet of 1 mm thickness. From this sheet, foils (dimensions 1 x 20 x 15 mm^3) were cut. The surfaces of the foils were ground and polished. Results of the chemical analysis of the cast alloy are shown in Table 1.

The foils were encapsulated in an Ar-filled quartz tube and recrystallized at 750 °C for 30 min. After recrystallization an equiaxed ferritic microstructure with a grain size of 20-40 µm was obtained. A $(100)_{\alpha\text{-Fe}}$ texture occurred in the recrystallized specimens due to the prior rolling (see Fig. 1). For determining the N strongly bound in the nitrides (see section 3.1) of the nitrided Fe-1Cr-1Mo alloy, a 1 mm specimen was further cold-rolled down to a thickness of about 200 µm, in order to obtain a homogeneously through-nitrided specimen, and recrystallized. Before nitriding, the specimens were polished (last stage 1 µm diamond suspension) and cleaned, successively, with ethanol, acetone and isopropanol.

The foil specimens were nitrided in a vertical multizone quartz tube furnace (temperature accuracy ±1 K) in a flowing NH_3/H_2 gas mixture. High purity ammonia (>99.998 vol.%) and hydrogen (>99.999 vol.%) gases were used. The flow rates of the ammonia and hydrogen gases were adjusted with calibrated mass flow controllers to get a nitriding potential r_N of 0.1 $atm^{-½}$, $r_N = \frac{p_{NH_3}}{p_{H_2}^{3/2}}$, where p represents the partial pressure [20]. Nitriding was performed at 580 °C for total nitriding times in the range of 1 h to 504 h. For the denitriding treatments

at 450 °C, r_N was adjusted to 0.01 atm and the total denitriding time was 96 h. Note that under the employed nitriding conditions iron nitrides cannot develop (on the surface) upon nitriding pure iron [21]. The nitriding treatment was terminated by quenching the specimen into N_2-flushed water at room temperature. The Fe-1Cr-1Mo thin foils were weighed before nitriding, after nitriding and after subsequent denitriding using a Mettler Toledo XP56 microbalance with a nominal accuracy of ±1 µg. The weight of the (lighter) thin foil for denitriding experiments was tracked with a Mettler Toledo UMX2 microbalance with a nominal accuracy of ±1 µg. Due to a slight magnetism of the ferritic specimens, the actually measured values scattered by about ±0.003 mg. From the gain/loss in weight of the foils, the amount of N taken up/lost by the foils was calculated.

2.2. Microstructural Characterization

To identify the different nitride phases developed upon nitriding, X-ray diffractograms were recorded from the surface of the nitrided foil specimens using a PANalytical MPD diffractometer operating in Bragg-Brentano geometry, and applying Co-K_α radiation and a graphite monochromator in the diffracted beam. The diffraction-angle 2θ range of 10°-130° 2θ was scanned with a step size of 0.009° 2θ. During the measurement, the specimen was rotated around its surface normal to improve the crystallite statistics. For phase identification, the substance reference patterns in the ICDD database [22] were used. Rietveld refinement of the diffraction data for identification of a new ternary nitride was performed with the TOPAS (Bruker AG) software. A pseudo-Voigt function was employed for the peak shape [23], [24]. The height displacement of the specimen in the diffractometer circle [25] was determined from the positions of the four ferrite peaks in the measured 2θ-range.

For metallographic investigations, parts of the nitrided specimens were cut off normal to the specimen surface and a protective Ni plating was applied to these parts by electrodeposition in a Watts bath [26], [27]. Such Ni-plated pieces were embedded in Struers Polyfast. The embedded specimens were ground, polished (last stage 1 µm diamond suspension) and etched with 1 % Nital. A LEO 1530 VP scanning electron microscope (SEM) equipped with a field emission gun and an in-lens detector was employed in this study.

Elemental (Fe, N, Cr and Mo) concentration-depth profiles were recorded from the cross-sections employing a Cameca SX100 electron probe microanalysis (EPMA) system at 15 kV and a current of 100 nA. Characteristic X-ray emission peaks were measured and divided by the corresponding intensities obtained from standard samples of pure Fe (for Fe-K_β), pure Cr (for Cr-K_α), pure Mo (for Mo-L_α) and γ'-Fe_4N (for N-K_α). Elemental concentrations were calculated from the intensity ratios employing the $\Phi(\rho z)$ approach [28].

For TEM investigations of the microstructure, rectangular pieces from the nitrided foils (edge length 3 mm) were cut and ground to discs of about 3 mm diameter. The discs were ground mechanically, dimpled and Ar-ion milled (3 kV, 8° ion angle of incidence, approx. 2 h, liq.-N_2 cooling). In order to obtain isolated nitride particles for TEM-based phase analysis, a nitrided thin foil (thickness approx. 200 µm) specimen was suspended in a solution of 2 vol.% HCl, 50 vol.% water, and 48 vol.% ethanol and electrolytically dissolved at 1.6 V for about 1 h. In order to remove the nitride particles from the specimen surface, the specimen was sonicated in the same electrolytic solution after every 15 min of the electrolytic dissolution. The thus obtained solution containing nitride particles was centrifuged for 2 h and the solution was discarded. Subsequently, the residue was rinsed with distilled water and ethanol, by ultrasonically suspending the residue in the liquid concerned and subsequent

centrifuging. Finally, approx. 50 µl of a suspension of the residue, as produced by ultrasonic treatment in isopropanol, was placed onto a carbon-film for TEM analysis using a µl-syringe. After evaporation of the isopropanol, finely distributed nitride particles suitable for TEM analysis remained. A Zeiss 912 Omega TEM operating at an acceleration voltage of 120 kV and a Philips CM 200 TEM operating at 200 kV equipped with an EDAX energy dispersive X-ray (EDX) spectrometer were employed in this study.

2.3. Atom Probe Tomography

For APT analysis, the 1 x 20 x 15 mm^3 foils (cf. section 2.1) were ground to a thickness of 0.6 mm and prepared for nitriding as described in section 2.1. The nitriding times employed, at 580 °C and a nitriding potential of 0.1 $atm^{-½}$, were 72 h to obtain a homogeneous CP microstructure, and 216 h to obtain a homogeneous DP microstructure. After the nitriding treatment, the foil specimens were sliced into small "matchsticks" of dimensions 0.6 x 0.6 x 15 mm^3 by electrical discharge machining. The surfaces of the matchsticks were then ground and polished to dimensions of 0.5 x 0.5 x 15 mm^3 with SiC-paper up to a final grid of P4000 and cleaned, successively, in acetone and isopropanol.

The matchsticks were then polished into needle-shaped specimens for APT by a standard two-stage electro-polishing method using 25 % perchloric acid and acetic acid with a voltage between 12-18 V in the first stage, and in the second stage 2 % perchloric acid and 2-Butoxyethanol with a voltage between 6-8 V [29]. APT investigations were carried out using a Cameca Local Electrode Atom Probe (LEAP) 3000X HR. The specimens were analyzed in pulsed-laser mode, applying laser pulse energies of 0.2-0.4 nJ. The specimen temperature and pulse fraction rate were set as 50 K and 200 kHz, respectively. The elemental distribution maps and quantitative information of the local chemistry of the precipitates

were obtained from the reconstructed APT data by the Integrated Visualization & Analysis Software (IVAS) package which is based on the standard reverse projection algorithm [30]; for details see Ref. [29].

3. Results and evaluation

Upon nitriding an Fe-1Cr-1Mo alloy substrate, a nitrided zone develops in the surface adjacent region, as revealed by the more pronounced etching contrast of this region in light micrographs (LM) (cf. Ref. [19]). The nitride particles developing in the initially forming CP regions are too small to be revealed individually by LM or (conventional) SEM (see TEM analysis presented in section 3.1). Upon prolonged nitriding (after a time of the order of 10 hours at 580 °C), DP-regions develop in which a lamellar morphology of nitrides occurs which can be observed by LM and SEM.

3.1. Continuously precipitated nitrides; initial stages

X-ray diffractograms recorded from the surface of specimens nitrided at 580 °C for different times are shown in Fig. 1. After nitriding, all ferrite-matrix reflections have split into two peaks. The peak at lower diffraction angle emerges upon nitriding and is of higher relative integrated intensity after short nitriding times. With increasing nitriding time, the peak at higher diffraction angles increases in relative integrated intensity. No additional reflections pertaining to second (nitride) phases can be detected.

TEM bright-field (BF) micrographs reveal the initial formation of finely distributed, nano-sized platelets with their broad faces parallel to $\{100\}_{\alpha\text{-Fe}}$ lattice planes of the ferrite matrix (Fig. 2a). The corresponding $[001]_{\alpha\text{-Fe}}$ zone axis selected area electron diffraction patterns (SADPs) show, corresponding to the coherent nature of the nitride particles, pronounced streaking along $<100>_{\alpha\text{-Fe}}$ directions owing to the small size and the misfit strain perpendicular to these directions (i.e. perpendicular to the platelet faces; Fig. 2b). Upon slight tilting of the specimen out of the $[001]_{\alpha\text{-Fe}}$ zone axis intensity maxima can be discerned on the streaks in the SADPs of the nitrided Fe-1Cr-1Mo alloy (Fig. 2c) at the positions

expected for diffraction spots of a cubic NaCl-type nitride having a lattice parameter close to $\sqrt{2}$ times the lattice parameter of the ferrite matrix ($\sqrt{2} \cdot 2.8664\text{Å} = 4.054\text{Å}$); the lattice parameter of CrN is 4.14 Å (card 011-0065 in Ref. [22]), and that of γ-Mo_2N is 4.163 Å (card 025-1366 in Ref. [22]). The position of these intensity maxima with respect to the diffraction spots of the ferrite matrix is compatible with a Baker-Nutting OR [15] of nitride precipitates and matrix (see Fig. 2d)).

In order to find out, whether the precipitation of Cr and Mo has occurred either as separate binary nitrides or as a ternary mixed nitride, local composition analyses have been performed by APT. The spatial distribution of the elemental species found in the mass spectra is given in Fig. 3a. Evidently, the matrix is strongly depleted of the original alloying elements and the N-rich regions, i.e. the nitride platelets, are rich in both Cr and Mo. Iso-concentration surfaces enclosing regions of a combined Mo, Cr and N concentration larger than 4 at.% have been plotted for the analyzed tip to more or less separate the nitride particles from the matrix. These iso-concentration surfaces are presented in Fig. 3b, thereby highlighting the orientation and spatial distribution of the platelets. The morphology of the platelets is consistent with that observed by TEM (cf. Fig. 2 and Fig. 3a; due to the longer nitriding time of 72 h somewhat longer platelets occur in Fig. 3a (APT results) as after 6 h of nitriding (Fig. 2); as also follows from a direct comparison of the TEM micrograph after 72 h of nitriding (Fig. 9) with that after 6 h of nitriding (Fig. 2)).

Determination of the exact composition of the nitrides by APT can be problematic. The key limitations are:

(i) Peak overlap in the mass-to-charge-state ratio spectrum can potentially occur for N^+ and N_2^{2+}, although this is expected to be limited. More significant is the peak overlap between N_2^+ and Fe^{2+} in the spectrum [31], [32]. Close inspection of the mass spectrum originating from the nitrides alone (i.e. the volume inside the iso-concentration surfaces of 4 at.% Cr+Mo+N) indicates that the peak ratios at 28, 28.5 and 29 Da follow the natural abundances of the isotopes of Fe. It is therefore concluded that no significant evaporation of nitrogen could be detected in the form of N_2^+.

(ii) Recent studies [33], [34] have shown that lateral surface diffusion of substitutional and interstitial atoms on the APT tip may affect the reconstruction of their original location on the tip thereby leading to inaccuracy in the determination of the composition of (small) second phase regions by APT. The electric field employed in the APT experiment is adjusted to give a steady evaporation of the Fe-based matrix. Thus, the effect of surface diffusion of the (heavier) substitutional species is likely not prominent and the co-enrichment of Cr and Mo (in the nitride) is certainly real. However, because the (surface) diffusion of light elements is considerably faster than that of heavier elements, the determination of their original location in the APT tip is more severely influenced by surface diffusion and quantitative determination of the N content of matrix and/or precipitates can be seriously affected. However, with reference to results in Ref. [34], the current experiments provide no evidence of significant surface migration of N.

(iii) The local magnification effect (LME) in APT can limit both spatial and chemical resolution in the analysis of precipitates within numerous alloy systems. Elements

within the nitrides have a higher evaporation field than Fe in the surrounding matrix, i.e. a higher electric field must be applied to evaporate these nitride constituents from the surface of the APT tip, as compared to Fe. Thus, the preferential evaporation of the surrounding ferrite matrix, as compared to the evaporation of precipitates, results in a change of the shape of the surface of the tip in the vicinity of the platelets. This, in turn, leads to aberrations in the trajectories of ions emitted from these regions, which affects the spatial resolution of their reconstructed positions in the 3D APT image. Furthermore, the size and shape of the precipitates and their orientation in the specimen can influence the aberrations of the trajectories and thus the severity of the LME. For the very fine platelets in the current alloy, LME may therefore lead to erroneous detection of large amounts of Fe in the platelets (see Table 2). Earlier atom probe field ion microscopy (APFIM) studies of nitrided Fe-Mo alloys [14], [35] also suggested the presence of considerable amounts of Fe in Mo-nitrides[1], whereas a study of nitrided Fe-Mo alloys based on Mössbauer spectroscopy [36] could not at all detect Fe in the nitrides. Furthermore, the aberrations by LME affect the observed shape of the precipitates: the width of the platelets appears thicker in Fig. 3a (APT) than in Fig. 2a (TEM).

[1] Investigations of nitrided Fe-Cr alloys by HRTEM-EDX have also led to the claim of the presence of Fe in "CrN", see Ref. [85]. However, also this conclusion is doubtful as the (scattered) electron beam generating the X-rays utilized in EDX analysis, will always excite Fe atoms from the ferrite matrix surrounding the precipitates, even if there would be no matrix above or below the precipitate in the TEM foil.

The above discussion implies that the APT data do not allow a definitive conclusion about the whether or not presence of Fe in the precipitates. However, this limitation does not affect the accuracy of the value determined for the atomic *ratio* of Cr and Mo content in the precipitates. The measured atomic Cr:Mo ratio is approximately 1:0.9, as expected for an alloy containing equal atomic amounts of Cr and Mo (cf. section 2.1). Hence, from the above results and discussion it is concluded, at this stage of the analysis, that the developed, cubic NaCl-type nitrides can be described as ternary nitrides of composition $(Cr_{½},Mo_{½})N_x$. Regarding the value of *x* and the effect of the possible presence of Fe in the nitride on the N-content, see in particular the next paragraph.

The precise stoichiometry of the developed ternary nitride was obtained as follows. A thin foil of Fe-1Cr-1Mo alloy (weight before nitriding: 471.953 mg) was nitrided to full saturation (12 h at 580 °C) such that no further N-uptake occurred and before a significant (aging induced) DP reaction could take place (see section 3.2). Next, this specimen was denitrided (96 h at 450 °C) to remove all less strongly bonded N, i.e. the dissolved N and the excess N adsorbed on the platelet faces (for details about excess N see Ref. [37]), i.e. the N which is not strongly bound in alloying element nitrides[2] (weight after denitriding 473.778 mg; with the accuracy of the weigth measurement (see section 2.1) this gives an error in the

[2] This treatment is the first step of a so-called absorption-isotherm analysis; see e.g. Ref. [41]. Denitriding of previously nitrided Fe-Mo specimens in pure, flowing H_2-atmosphere eventually causes all N to leave the specimen [36], i.e. the N-content becomes zero. This is a result of the low stability of Mo nitrides (see section 4). This effect can be prevented by applying a very low nitriding potential ($r_N = 0.01$ atm$^{-½}$; see section 2.1) to stabilize the nitrides. This nitriding potential will also lead to a very small amount of N dissolved in ferrite

N-content of ±0.003 at.%N). The N-content left in such a denitrided foil was 1.53 at.%, which indicates a strongly-bonded N to alloying-element (Cr+Mo) ratio of 0.765, i.e. a composition of $(Cr_{½},Mo_{½})N_{¾}$ for the ternary NaCl-type nitride platelets in the CP regions of this alloy. This composition is in line with the assumption of "a continuous series of solid solutions" [38] of CrN and γ-Mo_2N. This suggests that the composition of the ternary, mixed nitride is given by a weighted sum of the ratios Cr:N 1:1 and Mo:N 2:1. Thus, for the current alloy with Cr/Mo=1, it follows Cr:Mo:N=1:1:(3/2). This implies that the composition of the present ternary nitride can be represented as $(Cr_{½},Mo_{½})N_{¾}$. As a matter of fact, in a recent parallel investigation by our group of a series of Fe-Cr-Mo alloys of varying Cr/Mo-ratio, the N-content in the nitrided zone was found to comply with the above described rule for the composition of the mixed CP nitrides [39]. This result is a strong indication that indeed no significant amount of Fe is incorporated in these nitrides.

Already previous denitriding experiments of a number of through nitrided, ferritic, Fe-based binary alloys [40]–[43] and also a ternary Fe-Cr-Al alloy [44] indicated that the N-content remaining in the specimen after denitriding is compatible with the complete precipitation of all *Me* as *Me*N, or (Me_1,Me_2)N, respectively, implying (as above) that Fe is not significantly present in these nitrides. However, it might not be excluded that, if Fe is initially present in the nitrides, it may leave the nitrides during denitriding (if there exists a driving force for this effect). However, the mobility of Fe (in a nitride) at the relatively low denitriding temperature can be rather small. The initial incorporation of Fe into the nitrides would then

(about 0.003 at.% for the conditions employed here [86]), leading to a very slight, negligible overestimation of the N-content incorporated in the nitrides.

simply be the consequence of Fe not being able to “go out of the way” fast enough. For a related discussion and results from our group on the composition of nitrides developing upon nitriding of Fe-Cr-Al alloy, see Ref. [45].

3.2. Discontinuously precipitated nitrides; later stages

Continued nitriding of Fe-1Cr-1Mo alloy specimens, i.e. after completed initial precipitation of Cr and Mo in the form of coherent nitride platelets as discussed in section 3.1, leads to distinct microstructural change: starting from the grain boundaries, regions with a lamellar microstructure are formed by a discontinuous transformation mechanism (this reaction begins after a nitriding time of the order of 10 hours at 580 °C). An SEM micrograph showing such a discontinuously transformed region growing into the grain interior (i.e. into a CP region) is shown in Fig. 4. At this stage of the nitriding treatment, the platelets in the as yet untransformed CP-region have now become visible (see the right-hand side of the SEM micrograph), as they have experienced considerable coarsening due to the long nitriding (=aging) time.

An EPMA line scan crossing transformed DP regions and (as yet untransformed) CP regions of nitrided Fe-1Cr-1Mo alloy (see Fig. 5), indicates a larger N-content (approx. 2.4 at.%) for the DP regions as compared to the surrounding CP region (approx. 2.1 at.%). Recognizing the same amounts of Cr and Mo in the CP and DP microstructures, i.e. no alloying element redistribution occurs between CP and DP regions, it follows that the nitrides in the DP region contain more N than the nitrides in the CP regions. The additional N is supplied from the nitriding atmosphere during the ongoing nitriding reaction; cf. discussion on DP of MoN upon nitriding of binary Fe-1Mo alloy in Ref. [7].

The combined SEM, TEM and XRD analyses discussed below reveal the presence of three kinds of nitrides in the DP material:

(i) Straight, parallel, plate-like lamellae identified as $CrMoN_2$ (up to several µm long but very thin (about 10 nm thickness); see below) with broad faces parallel to $\{110\}_{\alpha\text{-Fe}}$ planes of the ferrite matrix (Fig. 4, Fig. 6, Fig. 8, Fig. 9, Fig. 10);

(ii) Spherical $(Cr,Mo)N_x$ particles in the ferrite lamellae between the $CrMoN_2$ lamellae (20-30 nm diameter; Fig. 4, Fig. 9, Fig. 11, Fig. 12);

(iii) Undulating platelets: small undulating platelets of α"-$Fe_{16}N_2$ with their broad faces overall parallel to $\{100\}_{\alpha\text{-Fe}}$ planes of the ferritic lamellae between the $CrMoN_2$ lamellae (Fig. 8, Fig. 12).

In the following, the structural and compositional details of the above types of nitrides are presented.

(i) DP-lamellae

X-ray diffractograms recorded from the surface of a Fe-1Cr-1Mo alloy specimen nitrided for prolonged treatment time (Fig. 6) show the presence of reflections of a new phase, in addition to the ferrite-matrix reflections, which emerged upon progress of the CP → DP transition.

Comparison of the new reflections with diffraction patterns of known phases of the Fe-Cr-Mo-N system (see overview of the Fe-Cr-N, Fe-Mo-N and Cr-Mo-N systems given in section 4) to identify the developed nitrides was unsuccessful. However, the positions of the new peaks are close to those expected for $CrWN_2$ [46]. It has been suggested [47], that Mo can partially substitute W in the layered $CrWN_2$ structure, but pure $CrMoN_2$ was not

synthesized until now (in an investigation of the precipitate phases forming in high-temperature steel materials [48], a ternary, layered, hexagonal Cr-Mo-nitride was proposed, although not fully characterized). Against this background, the crystal-structure data of $CrWN_2$ [46], with the W atoms fully substituted by Mo atoms, was used as a starting point for the Rietveld refinement of the lattice parameters of the accordingly proposed $CrMoN_2$ phase. The atomic positions of Cr, Mo, and N in $CrMoN_2$ were not refined, as the $CrMoN_2$ reflections are very weak in the diffraction pattern of the (bulk)[3] nitrided specimen (Fig. 6). The results of the fitting are shown in Table 3: the presence of such a $CrMoN_2$ phase is compatible with all but one of the new reflections (see Table 3 and Fig. 6); this very small unindexed reflection close to the 200 ferrite reflection in Fig. 6 could originate from a NaCl-type cubic nitride. This would suggest that not all $(Cr_{½},Mo_{½})N_{¾}$ (the CP nitride (cf. section 3.1)) has transformed to $CrMoN_2$ (the DP nitride). This is the case indeed; see (ii) below. The hexagonal crystal structure of $CrMoN_2$ is illustrated in Fig. 7. It is built of alternating densely packed Cr and Mo layers separated by densely packed N layers. In this structure, Cr is coordinated by N octahedra and Mo is coordinated by N-trigonal prisms.

TEM BF micrographs and corresponding SADPs of the DP regions (Fig. 8) show that the $CrMoN_2$ lamellae have their broad faces parallel to $\{110\}_{\alpha\text{-Fe}}$ ferrite-matrix lattice planes, indicating a habit plane different from that of the fine CP platelets which have their broad faces parallel to $\{100\}_{\alpha\text{-Fe}}$ ferrite-matrix lattice planes. The SADP shows diffraction spots of

[3] The isolated nitride powder (see section 2.2) showed a pronounced texture of the $CrMoN_2$ due to the plate morphology of the nitride lamellae (the plates lie on their faces, thus a strong 0001 texture occurs; see TEM results below), thereby prohibiting structural identification by Rietveld refinement of a corresponding X-ray diffractogram.

the lamellae in addition to the ferrite-matrix reflections (verified by dark field micrographs made employing only the additional spots (not shown)). These lamellae diffraction spots can be indexed according to the $CrMoN_2$ crystal structure as determined by the XRD analysis (see above). The position of the $000l$ spots of the hexagonal $CrMoN_2$ nitrides with respect to the 110 spots of the cubic ferrite matrix in SADPs with $[001]_{\alpha\text{-Fe}}$/ $[\bar{1}100]_{CrMoN_2}$ electron beam/zone axis indicates that closest-packed planes of nitrides and matrix are parallel, i.e. $\{0001\}_{CrMoN_2}||\{110\}_{\alpha\text{-Fe}}$.

Energy dispersive X-ray spectroscopy (EDX) spot analysis performed in the TEM of a freestanding lamella (Fig. 8b)) and of an electrolytically isolated lamella (cf. section 2.2; Fig. 10) shows that both lamellae contain the same amounts of Cr, Mo and N with a ratio of Mo/Cr>1, i.e. a higher amount of Mo than of Cr. Different values of the amounts of Cr, Mo and N in the nitride lamellae were obtained by evaluation of the EDX spectra if either the Mo K-lines or the Mo L-lines were considered, and therefore no quantitative composition data can be given. However, in both cases a Mo/Cr-ratio larger than one was obtained. As will be shown below, APT indirectly supports this indication of the TEM-EDX analysis, since characterization of the spherical particles shows that these particles exhibit a Mo/Cr-ratio smaller than one, as has to be expected if the lamellae indeed have a Mo/Cr-ratio larger than one and recognizing that in the alloy the Mo/Cr-ratio equals one.

(ii) Spherical precipitates

In SEM micrographs (Fig. 4), small particles are visible in the ferrite lamellae (between the $CrMoN_2$ lamellae). Close inspection of TEM-BF micrographs (Fig. 8a, Fig. 9, Fig. 10, and Fig. 11a and c) reveals the presence of these small, more or less spherical, particles as well. They appear to have no specific orientation relationship with the ferrite matrix; attempts to

obtain a low index electron-beam/zone axis SADP for these particles in the ferrite lamellae were unsuccessful. Therefore, the nitride particles (and nitride lamellae) were isolated from the matrix in order to increase the volume fraction of nitrides in a sample for TEM analysis, as described in section 2.2. The particles deposited onto the $CrMoN_2$ lamellae faces (Fig. 10) and those forming larger agglomerates (Fig. 11) were found to be roughly spherical. The SADPs of these agglomerates show diffraction spots on rings that are fully compatible with a NaCl-type crystal structure for the spherical particles (Table 4).

TEM-EDX analyses of some isolated particles (Fig. 11c) indicate the presence of Cr, Mo, and N with a ratio of Mo/Cr<1, i.e. the spherical particles contain more Cr than Mo. Different values of the amounts of Cr, Mo and N in the nitride lamellae were obtained by evaluation of the EDX spectra if either the Mo K-lines or the Mo L-lines were considered, and therefore no quantitative composition data can be given. However, in both cases a Mo/Cr-ratio larger than one was obtained. The Cr-enrichment in the spherical particles is confirmed by the elemental composition data obtained by the APT experiments shown in Fig. 12 and presented in Table 2: One spherical precipitate adjacent to the edge of the tip is shown in Fig. 12a; two spherical precipitates can be discerned in Fig. 12b. In order to separate the nitride particles from the matrix iso-concentration surfaces enclosing precipitate regions of a combined Mo, Cr and N concentration larger than 20 at.% were applied. The composition obtained of such defined precipitates is shown in Table 2.

(iii) Undulating platelets

The undulating platelets found in TEM BF micrographs (see arrows in Fig. 8a) resemble the morphology observed for α”-$Fe_{16}N_2$ in ferrite [49]–[51]. The metal atoms in this nitride are arranged in a tetragonally distorted bcc lattice [52]; the nitrogen atoms occupy c-type

octahedral interstices in an ordered way. These N atoms lead to only very weak superstructure spots in SADPs (note that the most intense, fundamental spots of α”-$Fe_{16}N_2$ overlap with those of ferrite-matrix spots [53]). APT shows that the undulating platelets contain N (are N-rich as compared to the matrix) and Fe, and that Cr and Mo have not been taken up in these undulating platelets (see Figs. 12 a) and b)).

α"-$Fe_{16}N_2$ is known to precipitate at room temperature or slightly elevated temperature from N-supersaturated ferrite [54], [55]. However, at the nitriding temperature of 580 °C employed in the current study, α”-$Fe_{16}N_2$ is unstable. Hence, the presence of α”-$Fe_{16}N_2$ precipitates within the Fe-lamellae is caused by aging (at RT) of the water-quenched (cf. section 2.1) nitrided specimens: quenching brought about retention of N-supersaturated ferrite at room temperature, and subsequent natural aging at room temperature causes the development of α”-$Fe_{16}N_2$ nitride particles.

4. Discussion

Upon nitriding of binary Fe-Cr alloys, initially *continuous precipitation* of finely distributed, nano-sized, cubic NaCl-type CrN nitride platelets, with a Baker-Nutting orientation relationship (OR) with the ferrite matrix, occurs [8], [9], [11]–[13]. The precipitation of CrN platelets is very fast, due to a high (negative) Gibbs energy of formation of CrN (per mole N_2)[4] (-129.1 kJ mol^{-1} at 580 °C (853 K) and 1 atm). During prolonged treatment time and given a sufficiently high Cr-content of the alloy (more than approx. 2 at.% Cr [9]), these fine precipitates can undergo a *discontinuous coarsening* reaction leading to the development of relatively small colonies/cells of alternating CrN and ferrite lamellae [9]–[13]. Under the high activity of N imposed by the nitriding atmosphere, CrN represents the thermodynamically stable Cr-nitride in nitrided binary, ferritic Fe-Cr alloys. No ternary phases have been reported for the Fe-Cr-N system [56].

Upon nitriding of binary, ferritic Fe-Mo alloys, initially continuous precipitation of thin but (as compared to nitrided Fe-Cr alloys) long, nano-sized, cubic NaCl-type γ-Mo_2N nitride platelets, with a Baker-Nutting OR with the ferrite matrix, occurs [7], [14]. Initially, the γ-Mo_2N platelets form very slowly which can be ascribed to the low Gibbs energy of formation of γ-Mo_2N (per mole N_2)[3] (-44.8 kJ mol^{-1} at 580 °C (853 K) and 1 atm); the volume

[4] The Gibbs energies of formation of the nitrides from the ferrite matrix ($\Delta G^f_{Me\mathrm{N},\alpha}$) presented here are determined by the Gibbs energies of formation of the nitrides from pure elemental Cr/Mo metal and N_2 gas ($\Delta G^f_{Me\mathrm{N}}$) (from Ref. [87]) and the activity of N at the current nitriding conditions (580 °C and 0.1 $atm^{-½}$) ($a_{\mathrm{N},\alpha}$) (from Ref. [88]) according to the formula $\Delta G^f_{Me\mathrm{N},\alpha} = \Delta G^f_{Me\mathrm{N}} - RT\ln(a_{\mathrm{N},\alpha})$. The contributions of the dissolution of Cr and Mo in ferrite are neglected. See Ref. [89] for more details of such calculation.

misfits of CrN and γ-Mo_2N with the ferrite matrix are similar (51 – 53 %)[5]. The thermodynamically stable nitride, hexagonal δ_3-MoN (volume misfit ~67 %), forms from the earlier developed nitride, upon prolonged nitriding by a *discontinuous precipitation* reaction leading to relatively large transformed regions of parallel alternating δ_3-MoN and ferrite lamellae [7]. For the system Fe-Mo-N, a cubic ternary η-Fe_3Mo_3N phase [57] and a WC-type hexagonal ternary $FeMoN_2$ phase [58] have been prepared by precursor synthesis from iron-molybdate powder ($FeMoO_4$, prepared from an aqueous solution) followed by reaction with pure flowing, gaseous ammonia at 650-700 °C.

The phase constitution of the ternary Cr-Mo-N system (at 1000 °C and 300 bar N_2) has been presented in Ref. [38]. Two types of nitride phases have been found:
i) a cubic, NaCl-type γ-Mo_2N/CrN phase conceived as "a continuous series of solid solutions" of CrN and γ-Mo_2N. The N-content of the corresponding mixed nitride was found to decrease from 50 at.% for pure CrN to 33 at.% for pure γ-Mo_2N with increasing Mo content. The same phase was also observed in investigations on Cr-Mo-N thin films (prepared under non-equilibrium conditions [59], [60]; and
ii) a hexagonal $(Cr,Mo)_2N$ phase, which can contain up to 55 at.% Mo at 1000 °C and 300 bar of N_2. Hexagonal, MoN-based phases [61]–[64] were not observed in the investigation of Ref. [38]. Other ternary nitrides of crystal structures different from the above mentioned

[5] The volume misfit $\frac{\Delta v}{v}$ of the nitride *B* with the ferrite matrix *A* is calculated from the molar volumes v_i according to $\frac{v_B - v_A}{v_A}$. Note that the molar volume used here must pertain to 1 mole *Me*. (i.e. for the B particle of composition MeN_N: the molar volume of MeN_N.)

ternary nitrides, and as found in other ternary transition metal nitride systems [46], [58], [65]–[67], have not been observed for the Cr-Mo-N system [38].

4.1. Continuous precipitation

Formation of ternary $(Cr_{½},Mo_{½})N_{¾}$ platelets

The present investigations on nitriding of Fe-1Cr-1Mo alloy showed that in the early stages of nitriding, similar to the case of nitrided Fe-Cr and Fe-Mo alloys, cubic NaCl-type $(Cr_{½},Mo_{½})N_{¾}$ nitride platelets develop (also with their broad faces parallel to $\{100\}_{\alpha\text{-Fe}}$ lattice planes of the ferrite matrix, and also with a Baker-Nutting OR with respect to the ferrite matrix). The nitriding time required to fully precipitate both Cr and Mo as NaCl-type ternary nitride in the ternary Fe-1Cr-1Mo alloy is much shorter than for the precipitation of Mo as NaCl-type binary nitride in the binary Fe-1Mo alloy [7]. The precipitation of Mo as nitride is evidently accelerated considerably by the presence of Cr. As indicated above for the binary systems, the binary NaCl-type nitrides CrN and γ-Mo_2N have considerably different Gibbs energies of formation (per mole N_2), which leads to the strongly differing precipitation kinetics of CrN (fast) and γ-Mo_2N (slow) for the respective binary systems upon nitriding. In the ternary system separate first, fast formation of Cr(-rich) nitrides and subsequent, slow formation of Mo(-rich) nitrides was not observed: instead, a ternary $(Cr_{½},Mo_{½})N_{¾}$-nitride developed.

The preference for the formation of the ternary nitride phase over the development of separate binary CrN and γ-Mo_2N phases upon nitriding of Fe-1Cr-1Mo alloy could suggest that the ternary nitride is thermodynamically preferred. The investigation of the ternary Cr-Mo-N system discussed above (Ref. [38]) and the results obtained from Cr-Mo-N thin films synthesized under various conditions (see e.g. Refs. [59], [60]) indicate that, under specific

conditions strongly different from those of the current experiments (see begin of section 4), development of the ternary, cubic NaCl-type (Cr,Mo)N_x nitride phase may be preferred thermodynamically over separate, binary cubic CrN and binary cubic γ-Mo_2N phases and then separate formation of binary nitrides is not to be expected. However, the cubic, NaCl-type ($Cr_{½}$,$Mo_{½}$)$N_{¾}$ phase formed in the present investigation, under the employed nitriding conditions, eventually transforms to the ternary hexagonal $CrMoN_2$ phase by a DP reaction, and thus does not represent a state of thermodynamic equilibrium.

The diffusion lengths of Cr^{51} ($\sqrt{2Dt}$ = 54 nm/h at 580 °C in Fe-based ferrite [68], with *D* and *t* representing the tracer, self-diffusion diffusion coefficient and the diffusion time) and in particular Mo^{99} ($\sqrt{2Dt}$ = 5 nm/h at 580 °C in Fe-based ferrite [69]) are relatively small at the employed nitriding temperature. It can therefore be suggested that the supposedly initially forming CrN incorporates Mo (note the different Gibbs energies of formation of CrN and γ-Mo_2N; see begin of section 4): the system accepts a lesser gain in (release of) chemical Gibbs energy and a slightly larger volume misfit (for binary CrN: 51%, for binary γ-Mo_2N: 53%) than as possible by the development of the separate binary nitrides, which, according to this interpretation, is kinetically obstructed. A similar reasoning, preferred formation of mixed nitrides based on kinetic constraints, was given previously for the mixed nitrides formed in nitrided ternary Fe-Cr-Ti [70] and Fe-Cr-Al [44], [71], [72] alloys. Indeed, the mixed, cubic NaCl-type (Cr,Ti)N and (Cr,Al)N nitrides, as holds for the mixed (Cr,Mo)N_x nitride of the present study as well, were found to be metastable in these systems: decomposition into the separate binary nitrides can take place at elevated temperature [72]–[74].

The nitride-precipitate platelets are finely distributed and are (largely) coherent with the ferrite matrix (see Fig. 2). Upon nitriding, initially the elastic accommodation of the

matrix/precipitate volume misfit causes long-range strains in the matrix which lead to an overall matrix expansion which causes the ferrite reflections to shift to lower diffraction angles [75]. A system composed of such fine nitride platelets and the ferrite matrix can diffract coherently, i.e. both matrix and nitride particles diffract as a single aggregate [76]. Furthermore, a compressive residual stress parallel to the surface results from the macroscopic misfit of the nitrided case and the unnitrided core causing a further peak shift to lower diffraction angles [77].

Upon continued nitriding, i.e. aging of the initially formed nitride platelets, in the precipitated regions not yet transformed by the DP reaction (cf. section 4.2; the DP reaction sets in after nitriding times of the order of 10 h at 580 °C) (mainly) increase of the precipitate size, i.e. continuous coarsening, occurs [78]. This is accompanied by plastic relaxation of the matrix/precipitate volume misfit and the development of a ferrite peak corresponding to the relaxed ferritic regions at higher diffraction angles [78]. In this stage, matrix and precipitates can diffract incoherently.

The matrix expansion, by elastic precipitate/matrix-misfit accommodation and macrostresses, and subsequent misfit relaxation are the origin of the presence of split ferrite reflections in the X-ray diffractograms (see Fig. 1): The lower angle peaks of the ferrite reflections originate from the expanded ferrite, representing coherent diffraction by the assembly ferrite matrix plus nitride platelets; the higher angle peaks of the ferrite reflections originate from the relaxed ferrite regions. Due to the ongoing relaxation, the contribution of the higher angle peak increases while that of the lower angle peak decreases with increasing nitriding time (see Fig. 1). The alloying element (Cr+Mo) content of the present alloy is not

sufficiently high to observe reflections of the coarsened, but still small[6], nitride platelets in X-ray diffractograms; yet, they are observed in TEM-SADPs (cf. diffractogram in Fig. 1 (for 6 h nitriding) and SADP in Fig. 2 (pertaining to 6 h of nitriding)).

4.2. Discontinuous precipitation

Under the currently employed nitriding conditions, the occurrence of a discontinuous reaction upon prolonged nitriding (of the order of 10 hours at 580 °C) with the accompanying formation of $CrMoN_2$ lamellae and the presence of $(Cr,Mo)N_x$ spherical precipitates in the ferrite lamellae, indicates that the initial, complete precipitation of Cr and Mo as $(Cr_{½},Mo_{½})N_{¼}$ nitride (cf. section 4.1) represents an intermediate, thermodynamically metastable (see discussion in section 4.1) state. The system likely passes through this intermediate stage due to a large nucleation barrier for the continuous precipitation of the (equilibrium) hexagonal $CrMoN_2$ phase in the ferrite matrix (see below). In the DP regions, no further phase changes were observed in the current study even after prolonged nitriding/aging up to 504 h at 580 °C.

Formation of ternary $CrMoN_2$ lamellae

Distinct formation of a lamellar microstructure by discontinuous coarsening (at the temperature considered) usually occurs in alloys with higher alloying element content and thus larger volume fraction of tiny, coherent nitride precipitates [9], [10] than in the current

[6] In the current alloy, at a depth of about 100 µm below the surface, the (initial) platelet dimensions after 1 h of nitriding are approximately 10 - 20 nm diameter and less than 1 nm thickness (TEM analysis performed in this project), and after 6 h of nitriding the dimensions have increased to 20 - 30 nm diameter and a few nm thickness (see Fig. 2).

alloy. For example, a DC reaction occurs in nitrided binary Fe-Cr alloys only with Cr contents above approx. 2 at% Cr. The higher the volume fraction of the tiny precipitates the larger the driving force for coarsening [9]. The reaction proceeds by rearrangement of atoms at and along moving grain boundaries [79], the reaction fronts, where interfacial diffusion governs the atomic transport, allowing DC to proceed at relatively low temperatures (as compared to continuous coarsening where atomic transport proceeds by volume diffusion) [76].

In systems where the initially forming nitride phase of the CP platelets does not represent the most stable nitride, as is the case of nitrided binary Fe-Mo alloys [7] and the present nitrided ternary Fe-Cr-Mo alloy (in contrast with nitrided binary Fe-Cr alloys), an additional chemical driving force operates for the DP reaction (as compared to a DC reaction), as additional *chemical* Gibbs energy is released by the formation of the more stable phase. Therefore, the occurrence of a discontinuous precipitation reaction can occur at a lower volume fraction of precipitates than for the occurrence of a discontinuous coarsening reaction.

From a comparison of the morphologies of the discontinuously formed regions (lamellae of $CrMoN_2$ and ferrite) of the present nitrided ternary Fe-Cr-Mo alloy with those of the DC regions developing upon prolonged nitriding of binary Fe-Cr alloys (see e.g. Ref. [10]) and the DP regions of binary Fe-Mo alloys [7] it follows that the morphology of the lamellar regions in the present, nitrided Fe-Cr-Mo alloy is similar to that observed in the nitrided Fe-Mo alloys, again suggesting that a discontinuous *precipitation* reaction occurs in the Fe-1Cr-1Mo alloy. This can be related to the structural similarities of $CrMoN_2$ and δ_3-MoN: both exhibit a hexagonal crystal structure and are oriented with their broad faces parallel to $\{110\}_{\alpha\text{-Fe}}$ ferrite lattice planes. However, due to the much faster initial precipitation of the cubic

nitride, here $(Cr_{½},Mo_{½})N_{¾}$, in the ternary alloy as compared to the binary Fe-Mo alloy, the time required to transform the specimen microstructure according to DP is much shorter in the ternary Fe-1Cr-1Mo alloy. The volume misfits of δ_3-MoN and $CrMoN_2$ with the ferrite matrix, are ~67 % and ~56 %, respectively. This distinctly smaller volume misfit of $CrMoN_2$ with the ferrite matrix can be an (additional) important factor for the relatively fast DP in the ternary alloys. Note that the volume misfit of the *hexagonal*, ternary nitride is much larger than that of the ternary cubic nitride (see section 4.1) making its nucleation in the ferrite matrix more difficult and, indeed, initially precipitation of *cubic* ternary nitride occurs (see section 4.1 and beginning of section 4.2).

A consequence of dissolution of (a part of; cf. discussion below on the spherical ternary nitrides) the initial, cubic nitride, followed by demixing, i.e. formation of the hexagonal nitride and ferrite at the moving boundary, carried by grain-boundary diffusion, is the establishment of a microstructure consisting of alternating ferrite and nitride lamellae with an incoherent interface (see also Refs. [11], [12], [76]). Consequently, incoherent diffraction of matrix and precipitates can be expected and indeed separate reflections of the nitride phase can be observed in the X-ray diffractograms and the SADPs (cf. Fig. 6 and Fig. 8).

Formation of spherical ternary $(Cr,Mo)N_x$

The DP reaction in nitrided binary Fe-Mo alloys leads to the full transformation of all initially formed γ-Mo_2N to δ_3-MoN [7]. Such full transformation to the DP nitride is not observed for the DP of $CrMoN_2$ from the initially formed $(Cr_{½},Mo_{½})N_{¾}$ in the nitrided ternary Fe-Cr-Mo alloys. While the DP reaction leads to a thermodynamically more stable microstructure, equilibrium in principle can*not* be attained at a reaction front migrating with a velocity larger than zero [80], [81]. Thus, part of the alloying elements cannot be taken up (in time) at the

reaction front into the developing $CrMoN_2$ lamellae. As an apparent consequence, more or less spherical $(Cr,Mo)N_x$ particles appear in the ferrite lamellae. The possible mechanisms of formation of these spherical precipitates can then be discussed as follows:

(i): All CP platelets dissolve at the DP reaction front. The Cr and Mo which cannot be incorporated (in time) into the forming $CrMoN_2$ lamellae remain dissolved and become incorporated in the ferrite lamellae where they subsequently *precipitate continuously* as $(Cr,Mo)N_x$. The precipitation of fine alloying element precipitates in the ferrite lamellae behind the discontinuous reaction front, was previously observed in Fe-Cr alloys with high Cr content [43]. However, the precipitation in the ferrite lamellae of the DC microstructure then occurred again in the form of fine platelets as in a CP microstructure. A spheroidization of these nitride platelets inside the ferrite matrix was not observed. As a matter of fact, the platelet shape of such cubic *Me*N nitrides is maintained even after long annealing times, also at elevated temperature (see e.g. Refs. [78], [82], [83]).

(iia): All CP platelets dissolve at the DP reaction front. The Cr and Mo which cannot be incorporated (in time) into the forming $CrMoN_2$ lamellae *precipitate at the reaction front* as cubic $(Cr,Mo)N_x$. Being in contact with two (parent and product) ferrite grains of different crystallographic orientations and confined between the forming $CrMoN_2$ lamellae, the $(Cr,Mo)N_x$ precipitates develop at the reaction front without a specific OR with the product ferrite (lamellae). Thus, the incoherent particles can assume a spherical shape to minimize their interfacial energy.

(iib): Some CP nitride platelets do not dissolve at, and are “overrun” by, the DP reaction front and *coarsen at the reaction front* by taking up the alloying elements that cannot be incorporated (in time) into the forming $CrMoN_2$ lamellae. Being in contact with two (parent and product) ferrite grains of different crystallographic orientations and confined between the forming $CrMoN_2$ lamellae, the $(Cr,Mo)N_x$ precipitates at the reaction cannot realize the preferred OR with the product ferrite (lamellae). Thus, the incoherent particles can assume a spherical shape to minimize their interfacial energy.

The above discussion suggests cases (iia) and (iib) to be more likely. The high magnification TEM micrograph in Fig. 9 shows both spherical and elongated particles in the ferrite lamellae in close proximity of the interface. Thereby it cannot be decided whether new spherical precipitates form at the interface (case (iia)) or whether former CP platelets are “overrun” and grow (case (iib)). Note that no further transformation of the spherical particles to the $CrMoN_2$ structure was observed, suggesting that both nitride phases, cubic and hexagonal, may be stable under the employed nitriding conditions after redistribution of alloying elements by the DP reaction.

5. Conclusions

The nitride development upon nitriding of Fe-1 at.%Cr-1 at.%Mo alloy can be summarized as follows:

1. Initially finely distributed, nano-sized, coherent, NaCl-type $(Cr_{½},Mo_{½})N_{¾}$ nitride platelets, exhibiting a Baker-Nutting OR with the ferrite matrix, develop. These mixed nitrides contain vacancies on the N sublattice equal to half the amount of the number of Mo atoms.
2. The $(Cr_{½},Mo_{½})N_{¾}$ nitride forms as a, kinetically preferred, intermediate precipitate as compared to the thermodynamically stable $CrMoN_2$ phase:
    i. The volume misfit with the matrix is much lower for $(Cr_{½},Mo_{½})N_{¾}$;
    ii. The diffusion lengths of (Cr and) especially Mo are small and incorporation of Mo in the possibly initially developing CrN (much larger release of Gibbs energy (per mole N_2) than for γ-Mo_2N) already leads to substantial release of Gibbs energy of the system.
3. Upon continued nitriding, i.e. upon aging, $CrMoN_2$ nitride forms as lamellae by a discontinuous precipitation mechanism. $CrMoN_2$ has a complex hexagonal crystal structure, as indicated by Rietveld refinement, of alternating, densely packed Cr and Mo layers separated by densely packed N layers.
4. The transformation of the $(Cr_{½},Mo_{½})N_{¾}$ platelets to $CrMoN_2$ lamellae during the DP reaction is not complete; remaining alloying element develops as cubic $(Cr,Mo)N_x$ as spherical particles contained in the ferrite lamellae (between the $CrMoN_2$-lamellae).

5. The atomic Mo content of the $CrMoN_2$ lamellae is somewhat larger than the atomic Cr content, in correspondence and consistent with an atomic Mo content of the spherical $(Cr,Mo)N_x$ particles somewhat smaller than the atomic Cr content, as indicated by both APT and TEM-EDX analyses.
6. The spherical $(Cr,Mo)N_x$ particles likely develop at the DP reaction front, either by nucleation or by growth from the initial $(Cr_{½},Mo_{½})N_{¾}$ platelets, and do not precipitate from the possibly remaining dissolved Cr, Mo, and N in the ferritic lamellae in the wake of the migrating reaction front.

Acknowledgements

The authors would like to thank Mr. W.-D. Lang for preparation of the TEM specimens, Mr. P. Kress for assistance with the nitriding experiments (all with Max Planck Institute for Intelligent Systems), Mrs. S. Haug for assistance with the EPMA experiments and Ms. S. Lacher for preparation of the APT matchsticks (both with Max Planck Institute for Solid State Research).

References (Will be adapted once the mansucript is finalized)

[1] *Metals Handbook, Volume 1: Properties and Selection: Irons, Steels, and High-Performance Alloys*. Materials Park: ASM International, 1990.

[2] E. Houdremont and H. J. Wiester, *Handbuch der Sonderstahlkunde*, 3rd edn., Springer Verlag, Berlin, 1956.

[3] Stahlinstitut VdEh (ed.), *Steel A Handbook for Materials Research and Engineering; Vol. 1: Fundamentals, and Vol. 2: Applications*, Springer Verlag and Verlag Stahleisen, Düsseldorf, 1984.

[4] C. H. Knerr, T. C. Rose, and J. H. Filkowski, *Gas Nitriding*, in *ASM Handbook, Volume 4: Heat Treating*, ASM International, Materials Park, 1991, pp. 387-409.

[5] E. J. Mittemeijer, *Fundamentals of Nitriding and Nitrocarburizing*, in *ASM Handbook, Volume 4A, Steel Heat Treating Fundamentals and Processes*, J. Dosset and G. E. Totten, eds., ASM International, Materials Park, 2013, pp. 619–646.

[6] E. J. Mittemeijer and M. A. J. Somers (eds.), *Thermochemical Surface Engineering of Steels*, 1st ed. Woodhead Elsevier, 2015.

[7] H. Selg, E. Bischoff, S. R. Meka, R. E. Schacherl, T. Waldenmaier, and E. J. Mittemeijer, *Molybdenum-Nitride Precipitation in Recrystallized and Cold-Rolled Fe-1 at. pct Mo Alloy*, Metall. Mater. Trans. A 44 (2013), pp. 4059–4070.

[8] B. Mortimer, P. Grieveson, and K. H. Jack, *Precipitation of nitrides in ferritic iron alloys containing Chromium*, Scand. J. Metall. 1 (1972), pp. 203–209.

[9] P. M. Hekker, H. C. F. Rozendaal, and E. J. Mittemeijer, *Excess nitrogen and discontinuous precipitation in nitrided iron-chromium alloys*, J. Mater. Sci. 20 (1985), pp. 718–729.

[10] R. E. Schacherl, P. C. J. Graat, and E. J. Mittemeijer, *Gaseous nitriding of iron-chromium alloys*, Z. Metallkde. 93 (2002), pp. 468–477.

[11] M. Sennour, P. H. Jouneau, and C. Esnouf, *TEM and EBSD investigation of continuous and discontinuous precipitation of CrN in nitrided pure Fe-Cr alloys*, J. Mater. Sci. 9 (2004), pp. 4521–4531.

[12] G. Miyamoto, A. Yonemoto, Y. Tanaka, T. Furuhara, and T. Maki, *Microstructure in a plasma-nitrided Fe–18 mass% Cr alloy*, Acta Mater. 54 (2006), pp. 4771–4779.

[13] G. Miyamoto, Y. Tomio, H. Aota, K. Oh-ishi, K. Hono, and T. Furuhara, *Precipitation of nanosized nitrides in plasma nitrided Fe-M (M = Al, Cr, Ti, V) alloys*, Mater. Sci. Technol. 27 (2011), pp. 742–746.

[14] J. Driver and J. Papazian, *The electron and field ion metallography of zones in nitrided Fe-Mo alloys*, Acta Metall. 21 (1973), pp. 1139–1149.

[15] R. G. Baker and J. Nutting, *The tempering of a Cr-Mo-V-W and a Mo-V steel*, Iron Steel Inst. Spec. Rep. 64 (1959), pp. 1–22.

[16] A. Molinari, T. Bacci, P. Campestrini, M. Pellizzari, and B. Tesi, *Plasma nitriding of Fe–Cr–Mo sintered steels*, Powder Metall. 42 (1999), pp. 119–125.

[17] A. Molinari, B. Tesi, T. Bacci, and T. Marcu, *Plasma nitriding and nitrocarburising of sintered Fe-Cr-Mo and Fe-Cr-Mo-C alloys*, Surf. Coatings Technol. 140 (2001), pp. 251–255.

[18] J. Kazior and C. Janczur, *Thermochemical treatment of Fe–Cr–Mo alloys*, Surf. Coatings Technol. 152 (2002), pp. 333–337.

[19] T. Steiner, S. R. Meka, E. Bischoff, T. Waldenmaier, and E. J. Mittemeijer, *Internal nitriding of ternary Fe-Cr-Mo alloys; nitride development*, Proceedings - European Conference on Heat Treatment and 21st IFHTSE Congress Munich (2014), pp. 53–61.

[20] E. J. Mittemeijer and J. T. Slycke, *Chemical potentials and activities of nitrogen and carbon imposed by gaseous nitriding and carburising atmospheres*, Surf. Eng. 12 (1996), pp. 152–162

[21] E. Lehrer, *Über das Eisen-Wasserstoff-Ammoniak-Gleichgewicht*, Z. Elektrochemie und Angew. Phys. Chemie 36 (1930), pp. 383–392.

[22] ICDD, *JCPDS-international Centre for Diffraction Data, PCPDFWIN*, JCPDS-international Cent. Diffr. Data, PCPDFWIN (2002).

[23] P. Thompson, D. E. Cox, and J. B. Hastings, *Rietveld refinement of Debye–Scherrer synchrotron X-ray data from $Al_2 O_3$*, J. Appl. Crystallogr. 20 (1987), pp. 79–83.

[24] R. A. Young and P. Desai, *Crystallite size and microstrain indicators in Rietveld refinement*, Arch. Nauk. o Mater. 10 (1989), pp. 71–90.

[25] A. J. C. Wilson, *Elements of X-ray crystallography*, Addison-Wesley, Reading, 1970.

[26] P. F. Colijn, E. J. Mittemeijer, and H. C. F. Rozendaal, *Light-Microscopical Analysis of Nitrided or Nitrocarburized Iron and Steels*, Zeitschrift für Met. 74 (1983), pp. 620–627.

[27] A. Wells, *Metallographic analysis of compound layers on ferritic nitrocarburized plain low carbon steel*, J. Mater. Sci. 20 (1985), pp. 2439–2445.

[28] J. L. Pouchou and F. Pichoir, *A new model for quantitative X-ray microanalysis*, Rech. Aerosp. 3 (1984), pp. 167–192.

[29] B. Gault, M. P. Moody, J. M. Cairney, and S. P. Ringer, *Atom Probe Microscopy*, Springer Science & Business Media, 2012.

[30] B. Gault, D. Haley, F. de Geuser, M. P. Moody, E. a Marquis, D. J. Larson, and B. P. Geiser, *Advances in the reconstruction of atom probe tomography data*, Ultramicroscopy 111 (2011), pp. 448–457.

[31] A. Martinavičius, R. Danoix, M. Drouet, C. Templier, B. Hannoyer, and F. Danoix, *Atom probe tomography characterization of nitrogen induced decomposition in low temperature plasma nitrided 304L austenitic stainless steel*, Mater. Lett. 139 (2015), pp. 153–156.

[32] M. Fonović, A. Leineweber, O. Robach, E. A. Jägle, and E. J. Mittemeijer, *The Nature and Origin of 'Double Expanded Austenite' in Ni-Based Ni-Ti Alloys Developing Upon Low Temperature Gaseous Nitriding*, Metall. Mater. Trans. A 46 (2015), pp. 4115–4131.

[33] B. Gault, F. Danoix, K. Hoummada, D. Mangelinck, and H. Leitner, *Impact of directional*

walk on atom probe microanalysis, Ultramicroscopy 113 (2012), pp. 182–191.

[34] G. Miyamoto, S. Suetsugu, K. Shinbo, and T. Furuhara, *Surface Hardening and Nitride Precipitation in the Nitriding of Fe-M_1-M_2 Ternary Alloys Containing Al, V, or Cr*, Metall. Mater. Trans. A 46 (2015), pp. 5011–5020.

[35] S. S. Brenner and S. R. Goodman, *FIM-atom probe analysis of thin nitride platelets in Fe-3 at.% Mo*, Scr. Metall. 5 (1971), pp. 865–870.

[36] G. P. Huffman and H. H. Podgurski, *Mössbauer study of nitrided Fe-Mo and Fe-Ti alloys*, Acta Metall. 23 (1975), pp. 1367–1379.

[37] M. A. J. Somers, R. M. Lankreijer, and E. J. Mittemeijer, *Excess nitrogen in the ferrite matrix of nitrided binary iron-based alloys*, Philos. Mag. A 59 (1989), pp. 353–378.

[38] P. Ettmayer, A. Vendl, and R. Kieffer, *Investigations of the Cr-Mo-N system*, High Temp. - High Press. 10 (1978), pp. 699–702.

[39] T. Steiner, S. R. Meka, E. Bischoff, T. Waldenmaier, and E. J. Mittemeijer, *Nitriding of ternary Fe-Cr-Mo alloys; role of the Cr/Mo-ratio*, submitted for publication.

[40] M. H. Biglari, C. M. Brakman, E. J. Mittemeijer, and S. Van Der Zwaag, *Analysis of the nitrogen absorption isotherms of cold-rolled Fe-2 at.% Al specimens with different AlN precipitate dimensions*, Philos. Mag. A 72 (1995), pp. 931–947.

[41] S. S. Hosmani, R. E. Schacherl, and E. J. Mittemeijer, *Nitrogen uptake by an Fe–V alloy: Quantitative analysis of excess nitrogen*, Acta Mater. 54 (2006), pp. 2783–2792.

[42] S. S. Hosmani, R. E. Schacherl, and E. J. Mittemeijer, *Nitrogen absorption by Fe-1.04at.%Cr alloy: uptake of excess nitrogen*, J. Mater. Sci. 43 (2008), pp. 2618–2624.

[43] S. S. Hosmani, R. E. Schacherl, L. Lityńska-Dobrzyńska, and E. J. Mittemeijer, *The nitrogen-absorption isotherm for Fe–21.5 at. % Cr alloy: dependence of excess nitrogen uptake on precipitation morphology*, Philos. Mag. 88 (2008), pp. 2411–2426.

[44] A. R. Clauss, E. Bischoff, S. S. Hosmani, R. E. Schacherl, and E. J. Mittemeijer, *Crystal Structure and Morphology of Mixed Cr1–x Al x N Nitride Precipitates: Gaseous Nitriding of a Fe-1.5 Wt Pct Cr-1.5 Wt Pct Al Alloy*, Metall. Mater. Trans. A 40 (2009), pp. 1923–1934.

[45] M. Akhlaghi, S. R. Meka, E. A. Jägle, S. J. B. Kurz, E. Bischoff, and E. J. Mittemeijer, *Low temperature nitriding of recrystallized and cold-rolled ferritic Fe-Cr-Al alloy*, Submitted for publication.

[46] K. S. Weil and P. Kumta, *Chemical Synthesis and Structural Investigation of a New Ternary Nitride, $CrWN_2$*, J. Solid State Chem. 128 (1997), pp. 185–190.

[47] K. S. Weil, P. Kumta, and J. Grins, *Exploration of Cation Substitution in the Layered Compound $CrWN_2$*, MRS Proc. 755 (2002), pp. 283–288.

[48] H. Beattie and F. Ver Snyder, *Microconstituents in High Temperature Alloys*, Trans. Am. Soc. Met. 45 (1953), pp. 397–428.

[49] P. Ferguson and K. H. Jack, *Quench-aging and strain-aging of nitrogen-ferrite*, Proc. Heat Treat. Conf. (1981), pp. 158–163.

[50] S. R. Meka, K. S. Jung, E. Bischoff, and E. J. Mittemeijer, *Unusual precipitation of amorphous silicon nitride upon nitriding Fe–2at.%Si alloy*, Philos. Mag. 92 (2012), pp. 1435–1455.

[51] K. Han, A. J. Böttger, H. W. Zandbergen, and E. J. Mittemeijer, *Microstructural changes during tempering of Fe-N martensite: formation of α''-nitride*, Philos. Mag. A 82 (2002), pp. 715–733.

[52] K. H. Jack, *Results of further X-ray structural investigations of the iron–carbon and iron–nitrogen systems and of related interstitial alloys*, Acta Crystallogr. 3 (1950), pp. 392–394.

[53] M. J. van Genderen, A. Böttger, R. J. Cernik, and E. J. Mittemeijer, *Early stages of decomposition in iron-carbon and iron-nitrogen martensites: Diffraction analysis using synchrotron radiation*, Metall. Trans. 24 (1993), pp. 1965–1973.

[54] L. Dijkstra, *Precipitation phenomena in the solid solutions of Nitrogen and Carbon in alpha Iron below the eutectoid temperature*, Trans. Am. Inst. Min. Metall. Eng. 185 (1949), pp. 252–260.

[55] E. J. Mittemeijer, A. B. P. Vogels, and P. Van Der Schaaf, *Aging at room temperature of nitrided α-iron*, Scr. Metall. 14 (1980), pp. 411–416.

[56] G. Effenberg and S. Ilyenko, *Landolt-Börnstein Group IV Physical Chemistry, Vol. 11D3: Ternary Alloy Systems: Cr-Fe-N*, Springer, Berlin, 2008.

[57] R. N. Panda and N. S. Gajbhiye, *Electronic and magnetic properties of Fe_3Mo_3N*, J. Alloys Compd. 256 (1997), pp. 102–107.

[58] R. N. Panda and N. . Gajbhiye, *Chemical synthesis and magnetic properties of nanocrystalline $FeMoN_2$*, J. Cryst. Growth 191 (1998), pp. 92–96.

[59] P. Hones, R. Sanjinés, F. Lévy, and O. Shojaei, *Electronic structure and mechanical properties of resistant coatings: The chromium molybdenum nitride system*, J. Vac. Sci. Technol. A Vacuum, Surfaces, Film. 17 (1999), p. 1024–1030.

[60] B. Gu, J. P. Tu, X. H. Zheng, Y. Z. Yang, and S. M. Peng, *Comparison in mechanical and tribological properties of Cr–W–N and Cr–Mo–N multilayer films deposited by DC reactive magnetron sputtering*, Surf. Coatings Technol. 202 (2008), pp. 2189–2193.

[61] A. Y. Ganin, L. Kienle, and G. V. Vajenine, *Synthesis and characterisation of hexagonal molybdenum nitrides*, J. Solid State Chem. 179 (2006), pp. 2339–2348.

[62] P. Ettmayer, *Das System Molybdän-Stickstoff*, Monatshefte für Chemie 101 (1970), pp. 127–140.

[63] A. Bezinge, K. Yvon, and J. Muller, *High-pressure high-temperature experiments on δ-MoN*, Solid State Commun. 63 (1987), pp. 141–145.

[64] C. L. Bull, P. F. McMillan, E. Soignard, and K. Leinenweber, *Determination of the crystal structure of δ-MoN by neutron diffraction*, J. Solid State Chem. 177 (2004), pp. 1488–1492.

[65] K. S. Weil and P. N. Kumta, *Synthesis of ternary transition metal nitrides using chemically complexed precursors*, Mater. Sci. Eng. B 38 (1996), pp. 109–117.

[66] P. S. Herle, *Synthesis of new transition metal nitrides, MWN_2(M=Mn, Co, Ni)*, J. Alloys Compd. 217 (1995), pp. 22–24.

[67] D. S. Bem and H.-C. Zur Loye, *Synthesis of the New Ternary Transition Metal Nitride $FeWN_2$ via Ammonolysis of a Solid State Oxide Precursor*, J. Solid State Chem. 104 (1993),
pp. 467–469.

[68] H. Bakker, *Landolt-Börnstein - Group III Condensed Matter, Vol. 26: Diffusion in Solid Metals and Alloys: 4 Self-diffusion in binary alloys and intermediate phases (tables): Ag-Al - Cu-Sn*, Springer Verlag, Berlin, 1990.

[69] H. Nitta, K. Miura, and Y. Iijima, *Self-diffusion in iron-based Fe–Mo alloys*, Acta Mater. 54 (2006), pp. 2833–2847.

[70] K. S. Jung, S. R. Meka, R. E. Schacherl, E. Bischoff, and E. J. Mittemeijer, *Nitride Formation and Excess Nitrogen Uptake After Nitriding Ferritic Fe-Ti-Cr Alloys*, Metall. Mater. Trans. A 43 (2011), pp. 934–944.

[71] K. S. Jung, R. E. Schacherl, E. Bischoff, and E. J. Mittemeijer, *Nitriding of ferritic Fe–Cr–Al alloys*, Surf. Coatings Technol. 204 (2010), pp. 1942–1946.

[72] A. R. Clauss, E. Bischoff, R. E. Schacherl, and E. J. Mittemeijer, *Phase transformation of mixed Cr_{1-x} Al_xN nitride precipitates in ferrite*, Philos. Mag. 89 (2009), pp. 565–582.

[73] P. H. Mayrhofer, H. Willmann, and A. E. Reiter, *Structure and phase evolution of Cr–Al–N coatings during annealing*, Surf. Coatings Technol. 202 (2008), pp. 4935–4938.

[74] R. Forsén, M. Johansson, M. Odén, and N. Ghafoor, *Decomposition and phase transformation in TiCrAlN thin coatings*, J. Vac. Sci. Technol. A Vacuum, Surfaces, Film. 30 (2012), pp. 061506-1–8.

[75] M. Akhlaghi, T. Steiner, S. R. Meka, A. Leineweber, and E. J. Mittemeijer, *Lattice-parameter change induced by accommodation of precipitate/matrix misfit; misfitting nitrides in ferrite*, Acta Mater. 98 (2015), pp. 254–262.

[76] E. J. Mittemeijer, *Fundamentals of Materials Science*, Springer, Berlin, 2011.

[77] E. J. Mittemeijer and U. Welzel (eds.), *Modern Diffraction Methods*, Wiley VCH, Weinheim, 2013.

[78] T. Steiner, M. Akhlaghi, S. R. Meka, and E. J. Mittemeijer, *Diffraction-line shifts and broadenings in continuously and discontinuously coarsening precipitate-matrix systems: coarsening of initially coherent nitride precipitates in a ferrite matrix*, J. Mater. Sci. 50 (2015), pp. 7075–7086.

[79] D. B. Williams and E. P. Butler, *Grain boundary discontinuous precipitation reactions*, Int. Mater. Rev. 26 (1981), pp. 153–183.

[80] J. W. Cahn, *The kinetics of cellular segregation reactions*, Acta Metall. 7 (1959), pp. 18–28.

[81] G. A. López, P. Zieba, W. Gust, and E. J. Mittemeijer, *Discontinuous precipitation in a Cu-4 . 5 at.-%In alloy*, Mater. Sci. Technol. 19 (2003), pp. 1539–1545.

[82] N. E. Vives Díaz, S. S. Hosmani, R. E. Schacherl, and E. J. Mittemeijer, *Nitride precipitation and coarsening in Fe–2.23at.% V alloys: XRD and (HR)TEM study of coherent and incoherent diffraction effects caused by misfitting nitride precipitates in a ferrite matrix*, Acta Mater. 56 (2008), pp. 4137–4149.

[83] B. Schwarz, S. R. Meka, R. E. Schacherl, E. Bischoff, and E. J. Mittemeijer, *Nitriding of iron-based ternary Fe–V–Si alloy: The precipitation process of separate nitrides*, Acta Mater. 76 (2014), pp. 394–403.

[84] M. H. Biglari, C. M. Brakman, and E. J. Mittemeijer, *Crystal structure and morphology of AlN precipitating on nitriding of an Fe-2at.% Al alloy*, Philos. Mag. A 72 (1995), pp. 1281–1299.

[85] C. Ginter, L. Torchane, J. Dulcy, M. Gantois, A. Malchère, C. Esnouf, and T. Turpin, *A new approach to hardening mechanisms in the diffusion layer of gas nitrided α-alloyed steels . Effects of chromium and aluminium: experimental and simulation studies*, La Metall. Ital. 7–8 (2006), pp. 29–35.

[86] J. Stein, R. E. Schacherl, M. Jung, S. R. Meka, B. Rheingans, and E. J. Mittemeijer, *Solubility of nitrogen in ferrite; the Fe–N phase diagram*," Int. J. Mater. Res. 104 (2013), pp. 1053–1065.

[87] I. Barin, *Thermochemical Data of Pure Substances*, Wiley-VCH Verlag GmbH, Weinheim, 1995.

[88] M. W. J. Chase, *NIST-JANAF Thermochemical Tables*, 4th edn., American Chemical Society, 1998.

[89] M. H. Biglari, C. M. Brakman, E. J. Mittemeijer, and S. van der Zwaag, *The kinetics of the internal nitriding of Fe-2 at. pct Al alloy*, Metall. Mater. Trans. A 26 (1995), pp. 765–776.

Figures

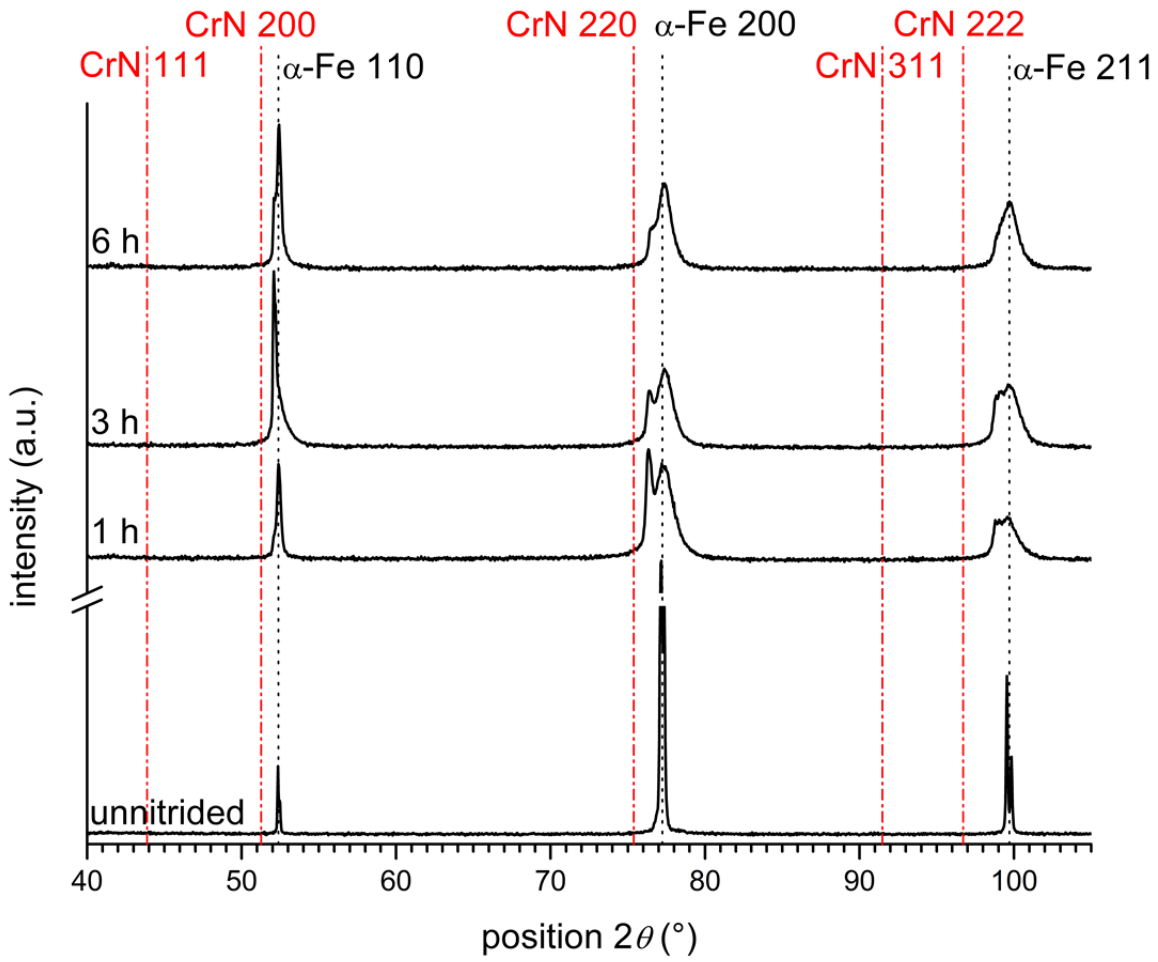

Fig. 1: XRD diffractograms (Co-K_α) recorded from the surface of Fe-1Cr-1Mo specimens nitrided at 580 °C with a nitriding potential of 0.1 $atm^{-½}$ for the nitriding times indicated; full patterns were normalized with respect to their integrated intensities. The reflection positions expected for CrN have been indicated by red dash-dotted lines, those for pure α-Fe by black dotted lines (see Ref. [19]).

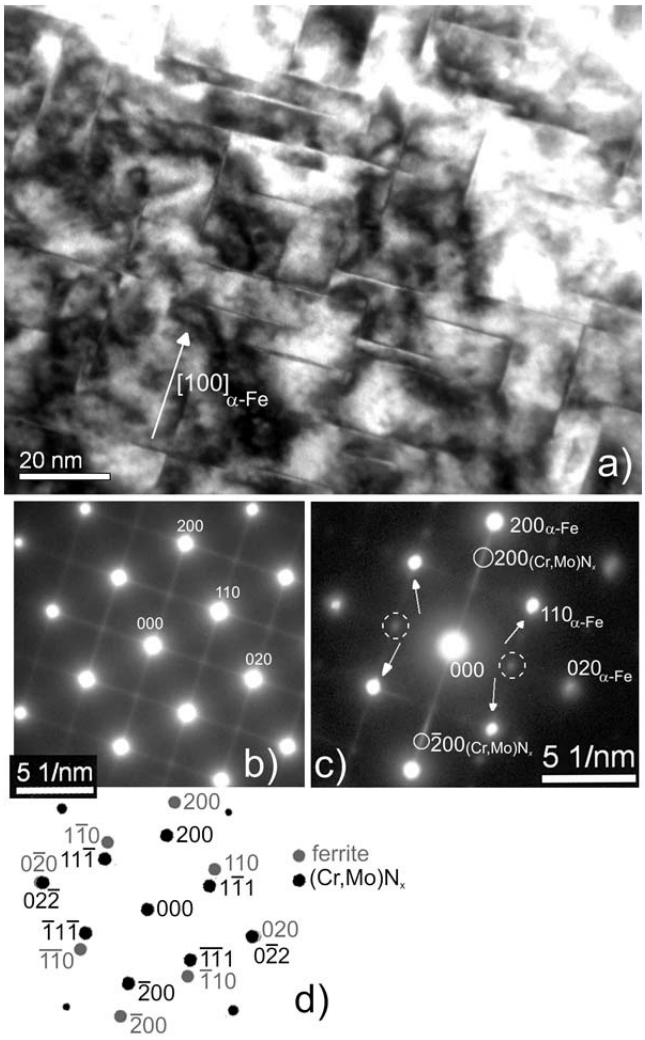

Fig. 2: a) TEM BF micrograph at a depth of 100 µm below the surface and b) the corresponding $[001]_{\alpha\text{-Fe}}$ electron beam direction/zone axis (ZA) SADP of the Fe-1Cr-1Mo specimen nitrided at 580 °C for 6 h with a nitriding potential of 0.1 $atm^{-½}$. Platelets occur along {001} habit planes of the ferrite matrix. In the $[001]_{\alpha\text{-Fe}}$ zone axis SADP distinct streaking along $<100>_{\alpha\text{-Fe}}$ directions is present. c) Slight tilting of the specimen out of the $[001]_{\alpha\text{-Fe}}$ zone axis reveals intensity maxima at $200_{(Cr,Mo)N_x}$ positions on the streaks. Expected $111_{(Cr,Mo)N_x}$ positions have been indicated with white arrows; dashed circled spots originate from magnetite Fe_3O_4 present on the TEM foil owing to unavoidable oxidation of the foil [84]. d) Schematic diffraction pattern of the ferrite matrix in $[001]_{\alpha\text{-Fe}}$ orientation and one variant of $(Cr,Mo)N_x$ in a Baker-Nutting orientation relationship (see Ref. [19]).

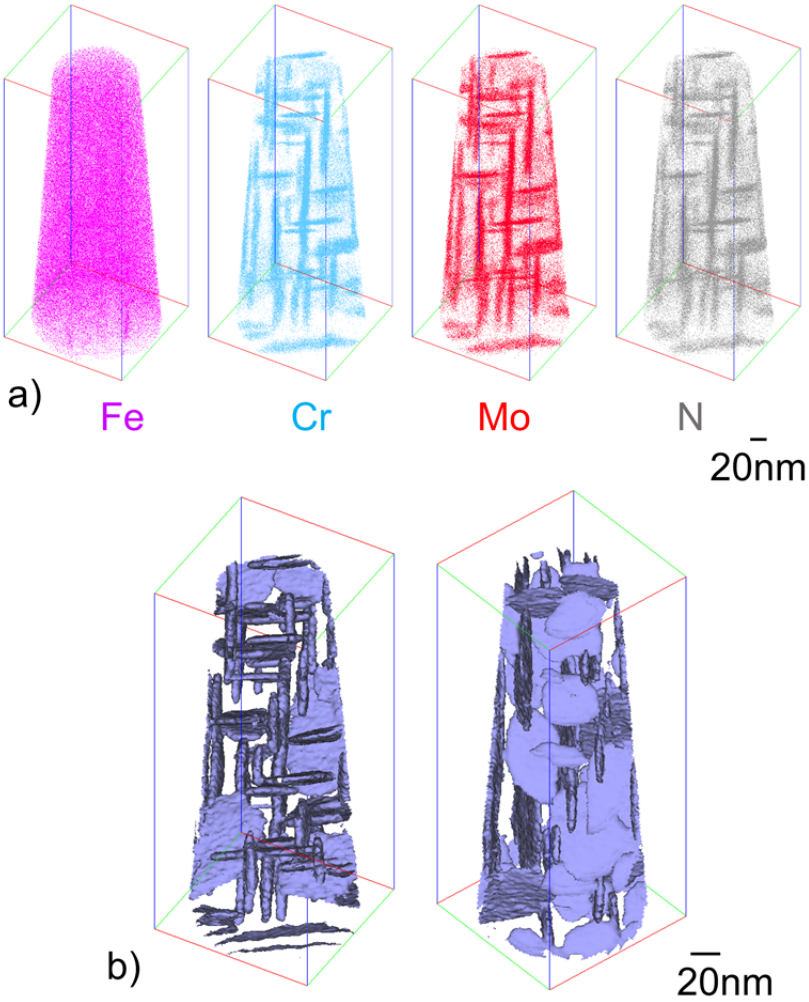

Fig. 3: a) Distribution of atomic species in an APT tip prepared from a Fe-1Cr-1Mo alloy specimen that was nitrided homogeneously at 580 °C for 72 h with a nitriding potential of 0.1 $atm^{-½}$. The size of the displayed box is 230 × 93 × 94 nm^3. Regions of increased contents of Cr, Mo, N species correspond to the ternary (Cr,Mo)N_x nitrides platelets evidenced by TEM. Due to restrictions in the resolution of the APT technique, the platelets appear thicker (and longer) than as indicated by the TEM analysis. b) Compositional iso-concentration surfaces of Cr+Mo+N = 4 at.%, i.e. within these surfaces the sum of the Mo, Cr and N contents exceeds 4 at.%, see Table 2. Left and right figures differ by rotation around the tip axis and inclination of the tip out of the viewing plane (see also the colored lines of the display box).

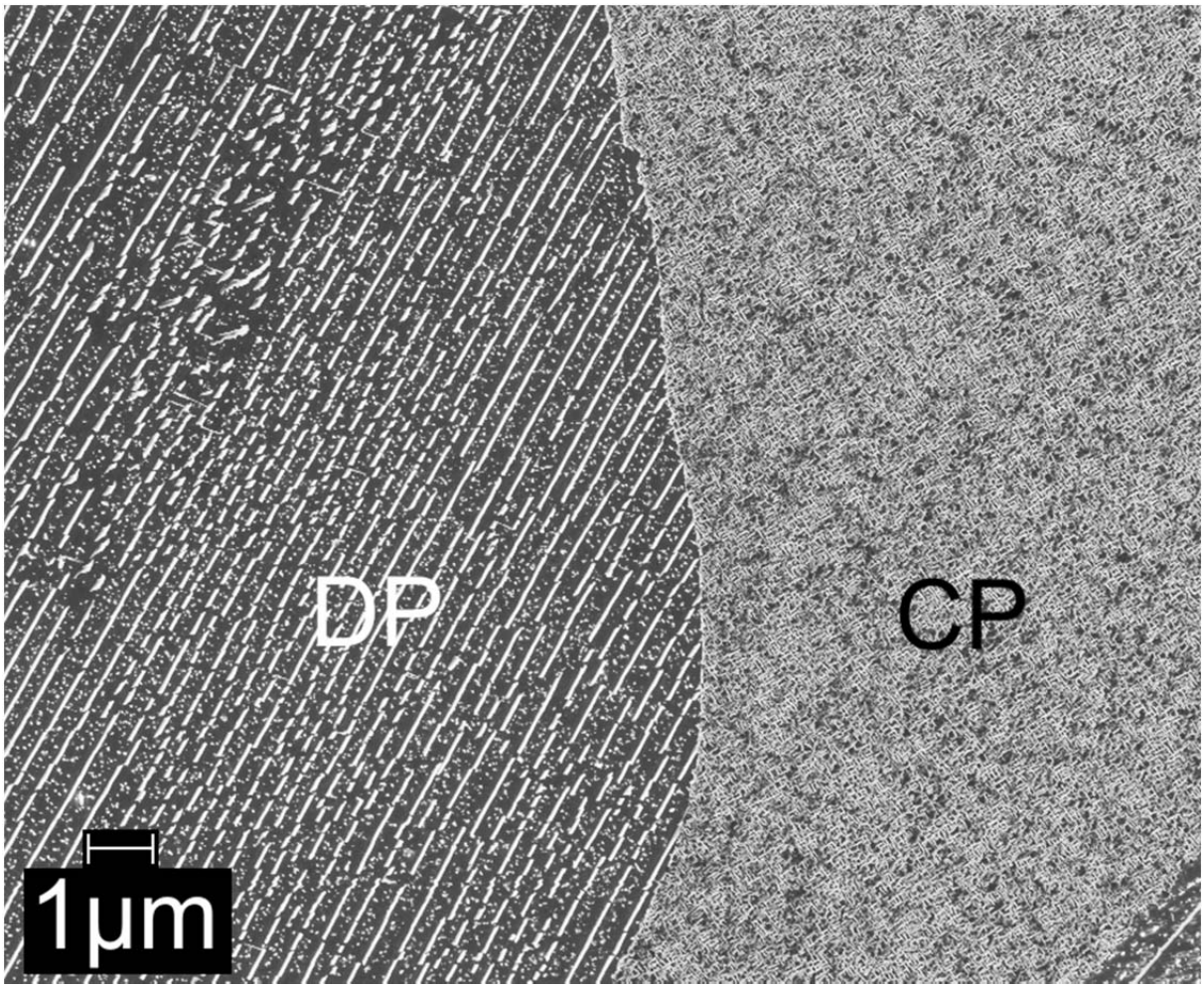

Fig. 4: SEM micrograph showing the microstructure as developed in the Fe-1Cr-1Mo alloy upon nitriding at 580 °C for 504 h with a nitriding potential of 0.1 $atm^{-½}$. The left part of the micrograph shows the lamellar microstructure: the $CrMoN_2$-nitride lamellae (white) and the ferrite lamellae (dark gray) with small spherical $(Cr,Mo)N_x$ nitride particles (light gray) in the ferrite lamellae resulting by the DP reaction occurring upon prolonged nitriding (aging). The right part of the micrograph shows the CP microstructure with relatively coarse (as compared to the initial stage of nitriding) $(Cr_{½},Mo_{½})N_{¾}$ platelets due to pronounced coarsening as a result of the prolonged time at elevated temperature.

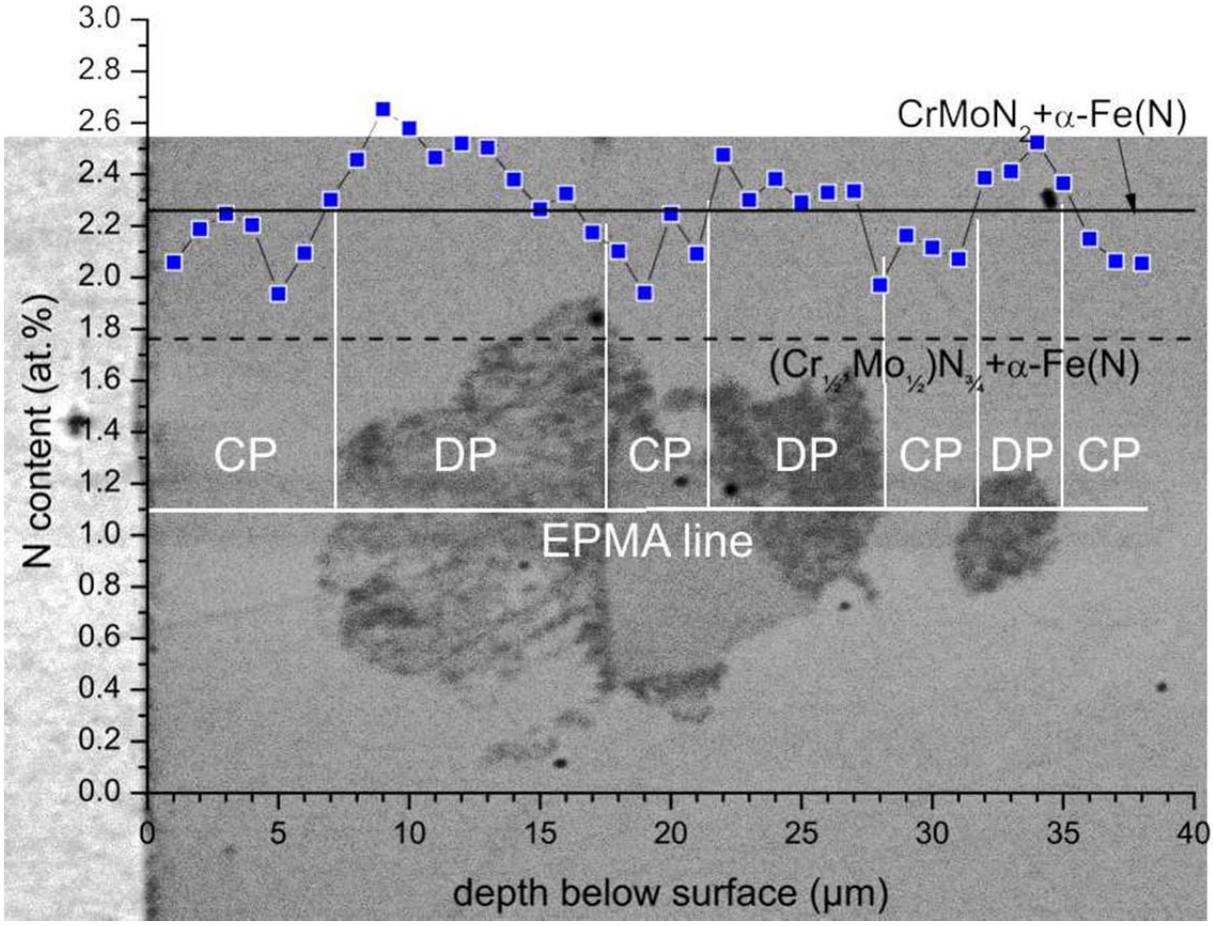

Fig. 5: EPMA line scan across a DP region in Fe-1Cr-1Mo alloy nitrided at 580 °C for 72 h with a nitriding potential of 0.1 $atm^{-½}$. The expected level of N-content for the case of precipitation of all Cr and Mo as $(Cr_{½},Mo_{½})N_{¾}$ plus the equilibrium N solubility of the ferrite matrix (1.76 at.% N; relevant for the CP microstructure) has been indicated by the dashed black line. The expected level of N-content for the case of precipitation of all Cr and Mo as $CrMoN_2$ plus the equilibrium N solubility of the ferrite matrix (2.23 at.% N; relevant for the DP microstructure) has been indicated by the full black line. Note that the presence of excess N particularly in the CP microstructure leads to a higher than expected N-content. The full horizontal white line indicates the position of the EPMA line scan; full vertical white lines indicate the positions of CP → DP reaction fronts crossed by the line scan.

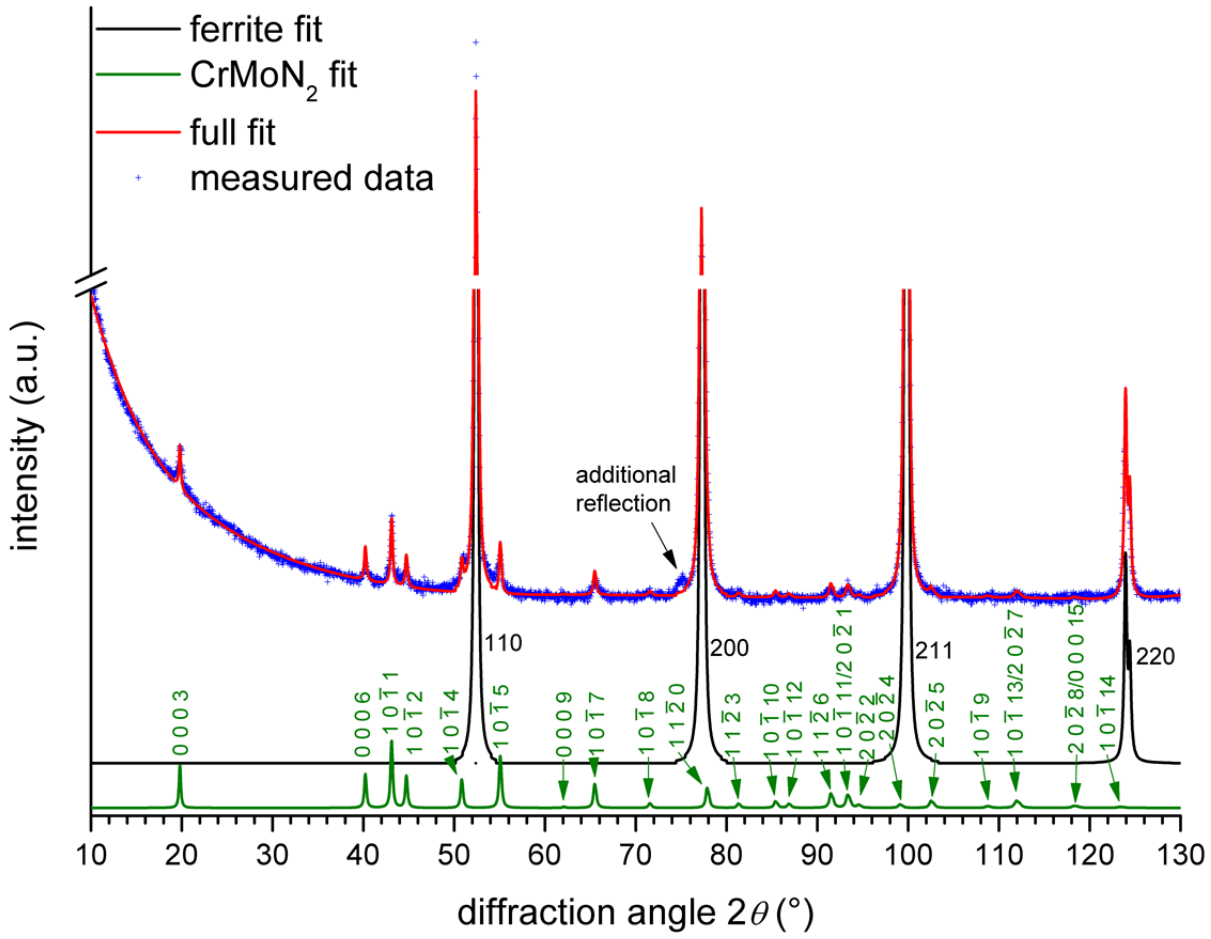

Fig. 6: XRD diffractogram (CoK_α) recorded from the surface of Fe-1Cr-1Mo alloy, nitrided at 580 °C for 504 h with a nitriding potential of 0.1 $atm^{-½}$. The fitted intensity curves for the ferrite (black) and $CrMoN_2$ (green) reflections are shown separately. The additional reflection at approx. 75° 2θ can be the NaCl-type 220 reflection of the coarsened spherical $(Cr,Mo)N_x$ particles in the DP ferrite lamellae (cf. Fig. 4).

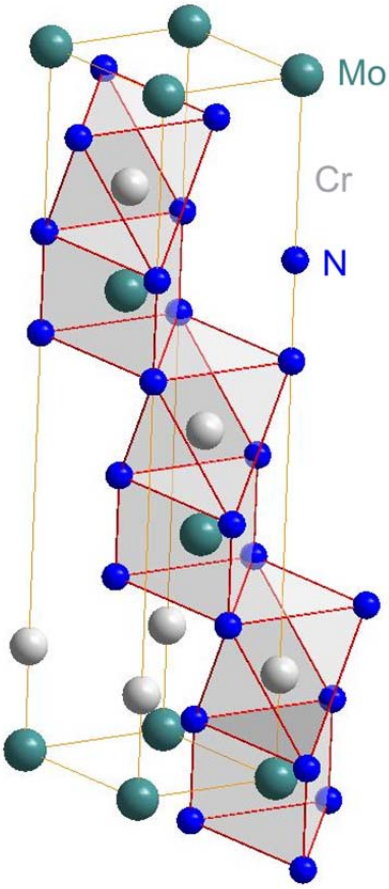

Fig. 7: Crystal structure of hexagonal $CrMoN_2$. Coordination of the metal atoms by N has been indicated by polyhedra. Cr shows an octahedral coordination by N and Mo shows a trigonal prismatic coordination by N. The structure consist of alternating densely packed layers of Cr and Mo which are separated by densely packed N layers in a stacking sequence $(aA_{Mo}aA_{Cr})(bB_{Mo}bB_{Cr})(cC_{Mo}cC_{Cr})$, where capital letters denote close packed layers of metal atoms and small letters denote close packed N layers.

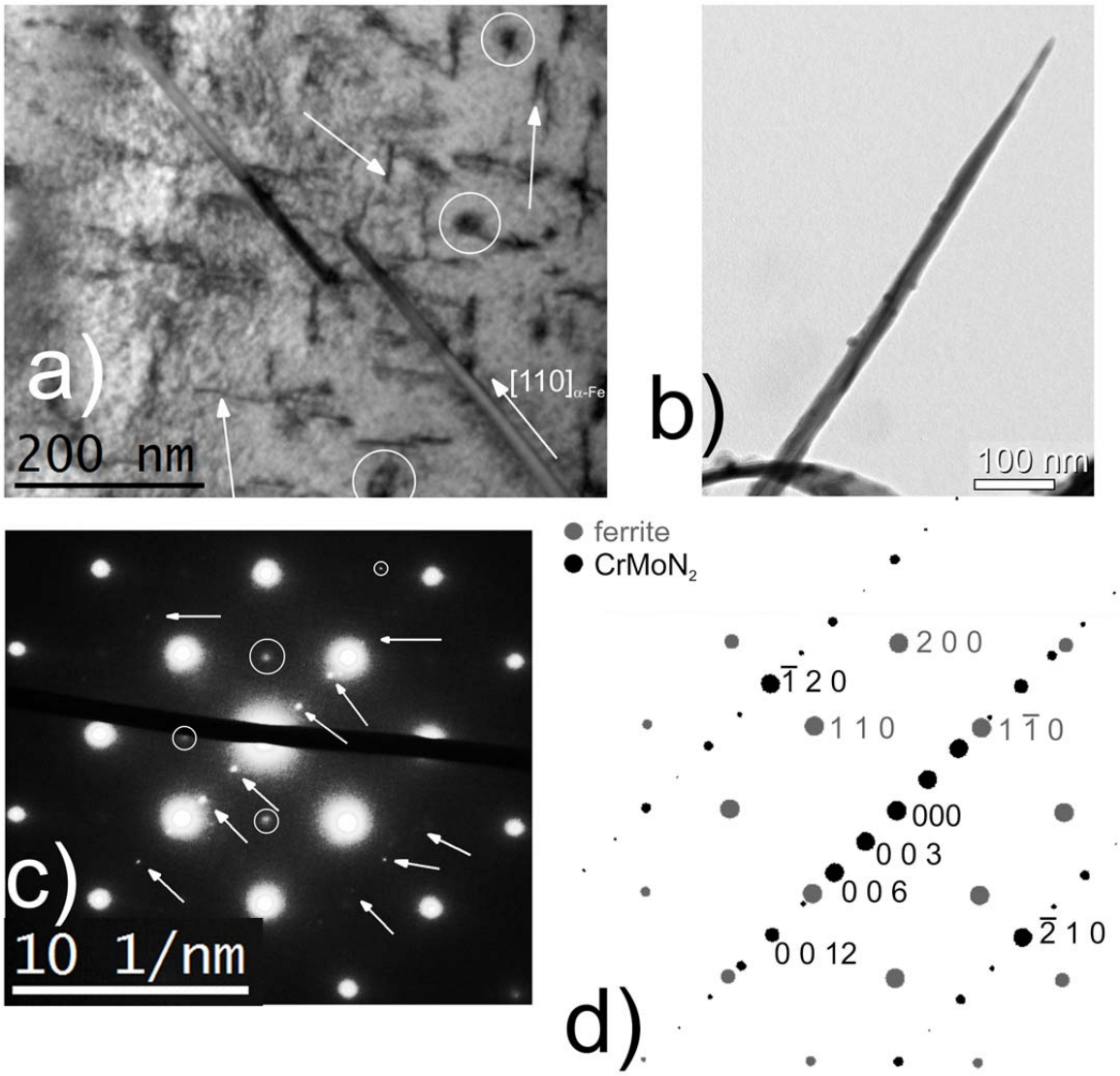

Fig. 8: (a) TEM bright field micrograph (BF) showing $CrMoN_2$ lamellae with their broad faces parallel to $\{110\}_{\alpha\text{-Fe}}$ ferrite lattice planes in Fe-1Cr-1Mo alloy nitrided at 580 °C for 72 h with a nitriding potential of 0.1 $atm^{-½}$. Some spherical (Cr,Mo)N_x particles in the ferrite lamellae have been indicated by white circles. Undulating appearing platelets in the ferrite lamellae (arrows), oriented along $\{100\}_{\alpha\text{-Fe}}$ ferrite planes, are α''-$Fe_{16}N_2$ precipitates formed in the nitrogen supersaturated (after quenching) ferrite lamellae upon aging at low (RT) temperatures [49], [50]. (b) Free-standing $CrMoN_2$ lamella employed for EDX analysis: a Mo/Cr-ratio larger than 1 was observed (see discussion in section 3.2). (c) SADP (electron beam/zone axis $[001]_{\alpha\text{-Fe}}$) of a). The arrows indicate spots belonging to the $CrMoN_2$ phase;

circled spots originate from unavoidable magnetite Fe_3O_4 present on the TEM foil. (d) Schematic diffraction pattern of the ferrite matrix and the $CrMoN_2$ nitride corresponding to a $[\ 1\bar{1}00\ ]_{CrMoN_2}$ / $[001]_{\alpha\text{-}Fe}$ zone axis. The arrangement of the spots indicates $(0001)_{CrMoN_2}||(110)_{\alpha\text{-}Fe}$.

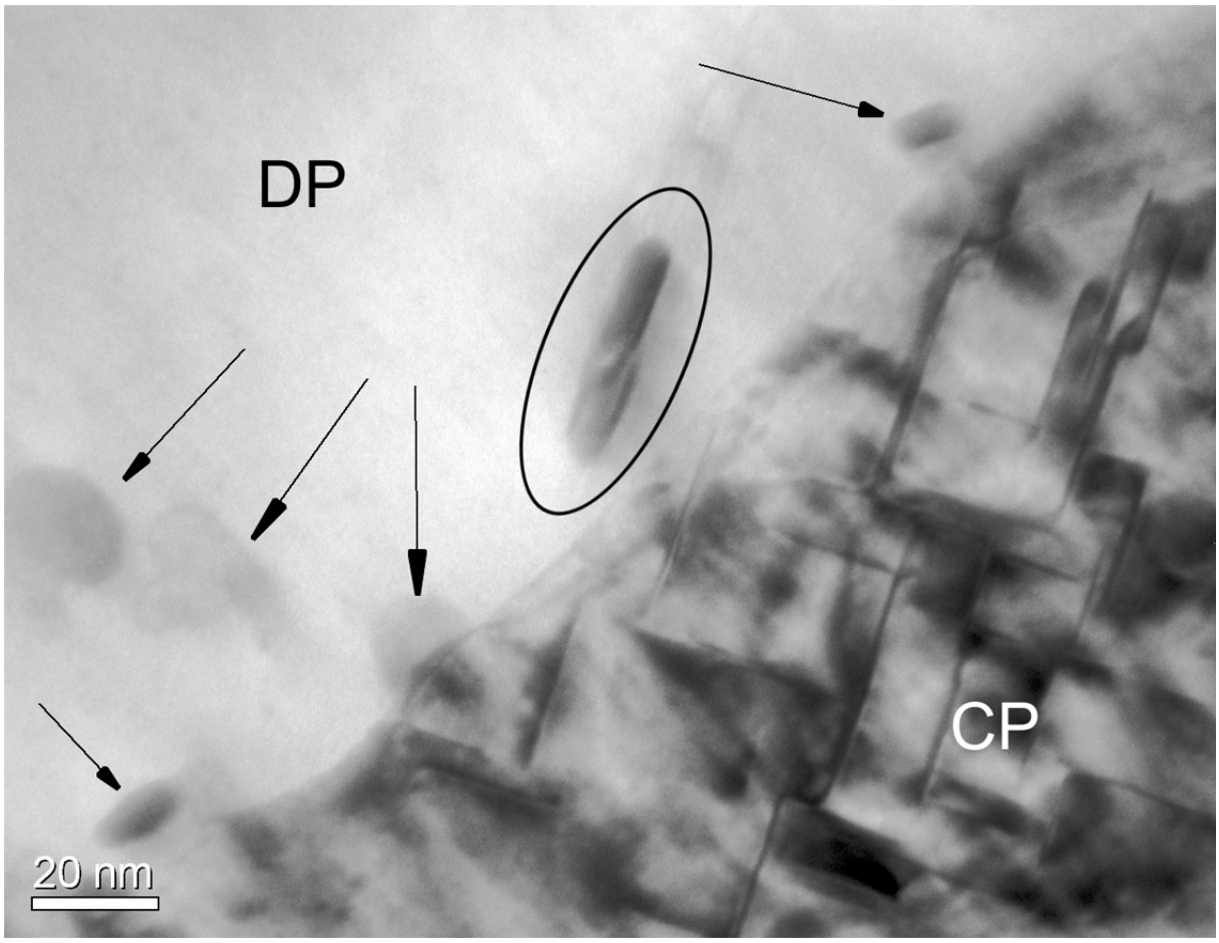

Fig. 9: TEM bright field (BF) micrograph at and around a CP/DP (ferrite lamella) interface in Fe-1Cr-1Mo alloy nitrided at 580 °C for 72 h with a nitriding potential of 0.1 $atm^{-½}$. Spherical particles have been indicated by arrows. Some spherical particles are visible very close to the interface. Black ellipse encloses an elongated particle with an elongation direction parallel to the long direction of a set of the former CP platelets. The electron-beam direction in the CP region is near to a $[001]_{\alpha\text{-Fe}}$, ferrite zone axis, whereas the electron-beam direction in the DP region (ferrite lamella) corresponds with a high index ferrite direction.

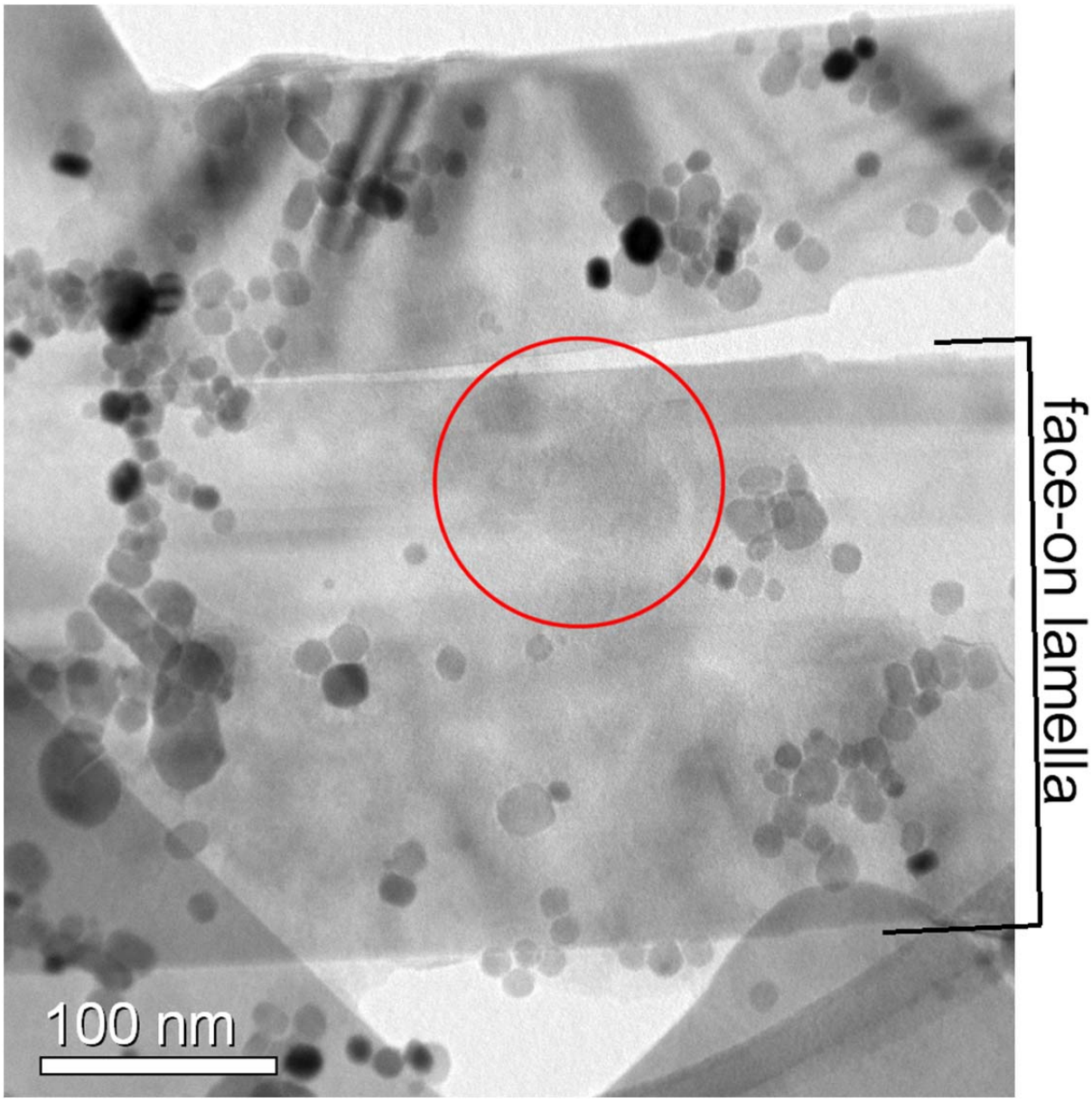

Fig. 10: TEM bright field (BF) micrograph of electrolytically isolated (i) $CrMoN_2$ lamella and (ii) spherical $(Cr,Mo)N_x$ particles. The (dissolved) specimen was a thin foil (thickness approx. 200 µm, cf. section 2.2) that was homogeneously nitrided at 580 °C for 72 h with a nitriding potential of 0.1 $atm^{-½}$ to have a fully DP microstructure. Spherical particles from the dissolved *ferrite* lamellae had deposited on the faces of the $CrMoN_2$ lamellae upon electrolytic dissolution. The red circle indicates the aperture position for EDX spot analysis: a Mo/Cr-ratio larger than 1 was observed (see discussion in section 3.2).

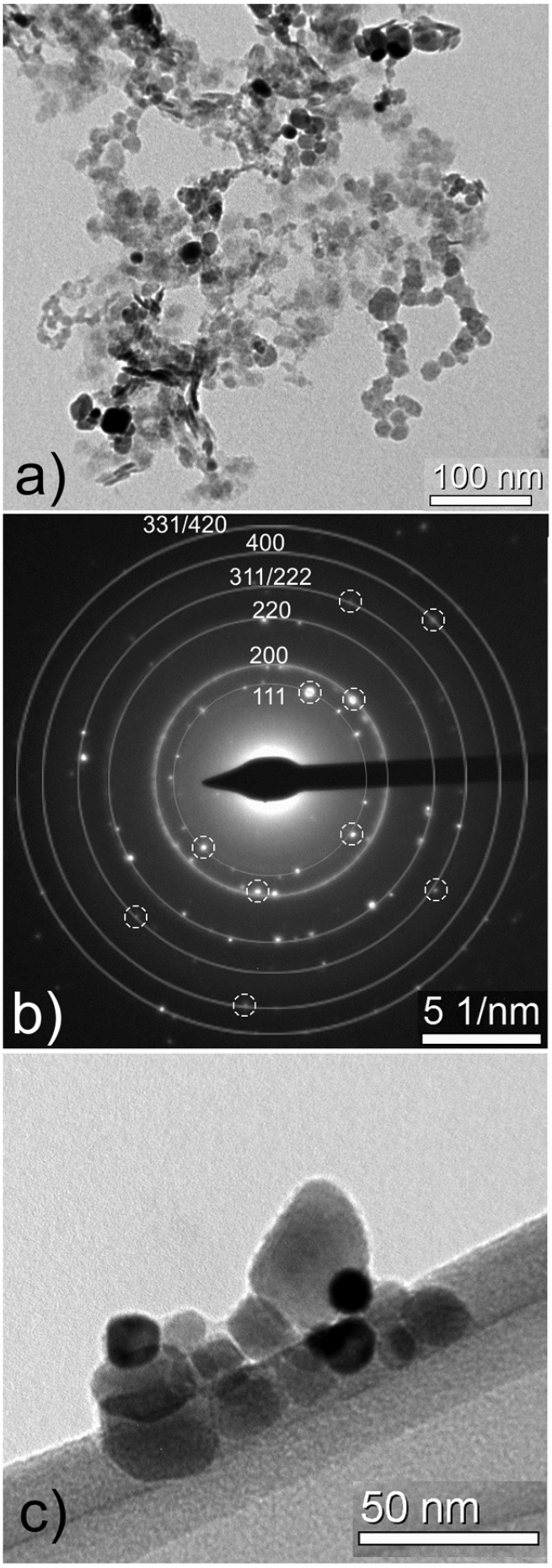
a)
100 nm
331/420
400
311/222
220
200
111
b)
5 1/nm
c)
50 nm

Fig. 11: (a) TEM bright field micrograph (BF) showing an agglomerate of spherical particles obtained by electrolytically dissolving the ferrite matrix. The (dissolved) specimen was a thin foil (thickness approx. 200 µm, cf. section 2.2) that was homogeneously nitrided at 580 °C for 72 h with a nitriding potential of 0.1 $atm^{-½}$ to have a fully DP microstructure. (b) The corresponding SADP. The diameters of the concentric rings can be indexed based on the NaCl-type crystal structure of $(Cr,Mo)N_x$. The corresponding d-spacings have been given in Table 4. The dashed white circles indicate some reflections of low and higher order (111 and 222 (ring 1 and 4) and 200 and 400 (ring 2 and 5); cf. Table 4). The more homogeneous appearance of the second ring (d-spacing approx. 2.07 Å) may originate from undissolved α-Fe in the agglomerate (d_{110}(α-Fe) is 2.0268 Å), or oxidation (of the nitride particles and/or the ferrite (see Fig. 2 and Fig. 8). As also strong spots occur along the ring, this is concluded to be also a d-spacing of the spherical $(Cr,Mo)N_x$ particles. (c) Smaller agglomerates of the spherical particles on which EDX analysis was performed: a Mo/Cr-ratio smaller than 1 was observed (see discussion in section 3.2). The grey band is the C-film (see section 2.2).

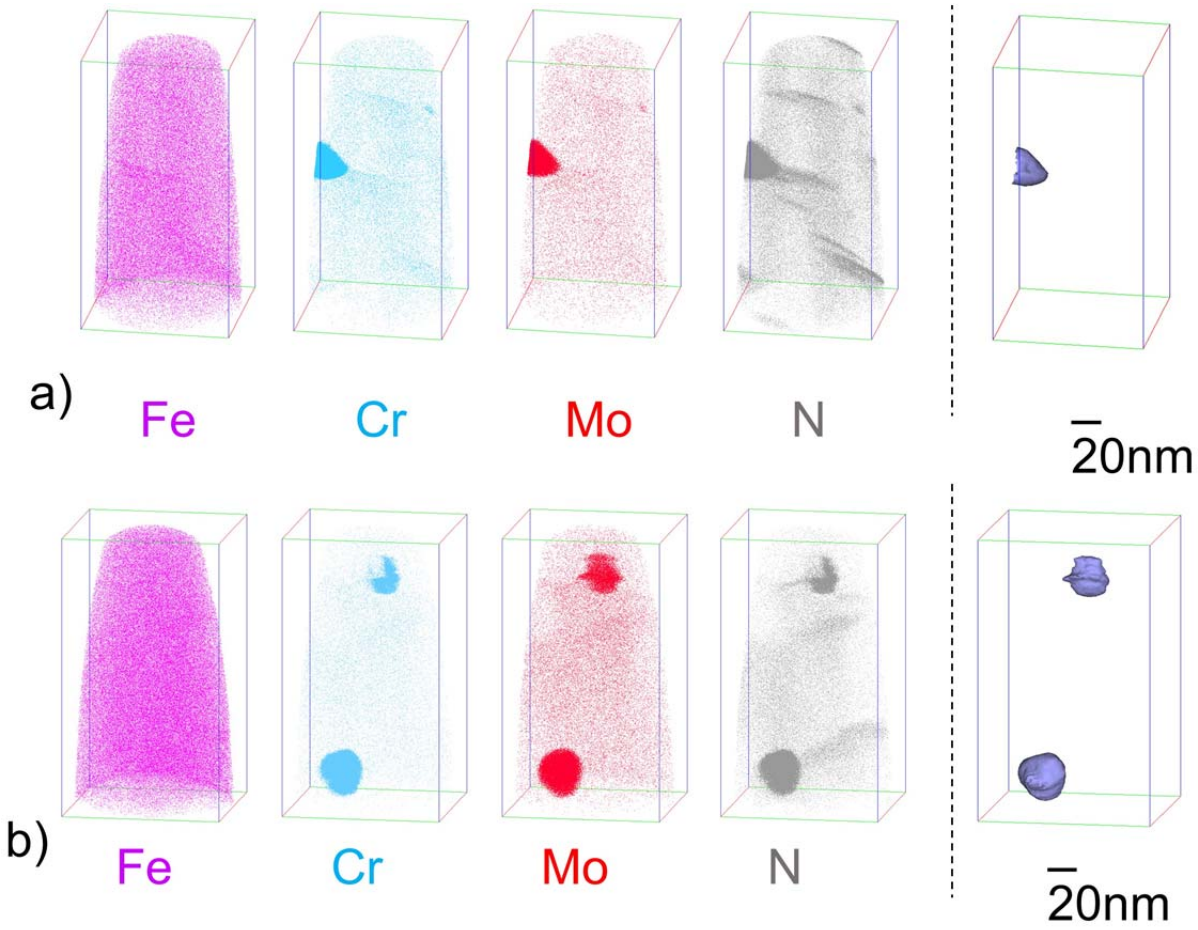

Fig. 12: (a) Distribution of atomic species (left) and compositional iso-concentration surfaces of Cr+Mo+N = 20 at.% (right) in an APT tip prepared from a (approx. 600 µm thick, c.f. section 2.3) Fe-1Cr-1Mo alloy specimen where the discontinuous precipitation reaction had (almost) completed after 216 h of nitriding at 580 °C with a nitriding potential of 0.1 $atm^{-½}$. The size of the displayed box is 164×86×86 nm^3. The region of increased contents of Cr, Mo and N species corresponds with either the tip (thin end) of a $CrMoN_2$ lamella or a spherical precipitate. Composition analysis indicates a higher content of Cr as compared to Mo in the nitride region (see Table 2). The N-rich regions, where neither Cr nor Mo are (significantly) enriched, correspond to the undulating α''-$Fe_{16}N_2$ platelets revealed by TEM. (b) A second APT tip of the same material containing two spherical precipitates and several undulating platelets. Composition of the particle enclosed by a red circle is given in Table 2.

Tables

Table 1: Composition of the Fe-1Cr-1Mo alloy used in this work. The Cr, Mo, Mn and Si contents were determined by inductive coupled plasma optical emission spectroscopy; the C content was determined by a combustion method; carrier gas hot extraction was applied for determination of the O and N contents.

element	Cr	Mo	Mn	Si	C	O	N	Fe
content [at. %]	1.01±0.01	0.98±0.01	<0.001	<0.02	0.010±0.001	0.021±0.004	<0.004	bal.

Table 2: Composition within iso-concentration surfaces containing different nitride particles as determined by APT in this study. The compositional analysis by APT is affected, especially, by the local magnification effect, which may lead to considerable, erroneous assignment of Fe from the surroundings to the nitrides (see section 3.1).

nitride precipitate	analysis method	Fe content (at.%)	Cr content (at.%)	Mo content (at.%)	N content (at.%)
CP-platelets	APT (Fig. 3b)*	89.7	3.45	3.00	3.82
DP-sphere	APT (Fig. 12a)°	31.5	26.8	11.0	30.8
DP-sphere	APT (Fig. 12b)°	28.7	30.4	9.45	31.4

*considering atoms inside the 4 at.% Mo-Cr-N-iso-concentration surface

°considering atoms inside the 20 at.% Mo-Cr-N-iso-concentration surface

Table 3: Structural data of and fitting results for the $CrMoN_2$ crystal-structure parameters. Atomic positions were not refined (see section 2.2).

refined structure data			
space sroup	R3m (160)		
a [Å]	2.8503(7)		
c [Å]	15.626(6)		
fitting criteria (figures of merit)			
R_{wp}	2.92		
R_{exp}	1.54		
GOF (=$\sqrt{\chi^2}$)	1.89		
atom positions [46]			
atom	x	y	z
Cr	0	0	0.825
Mo	0	0	0
N1	0	0	0.263
N2	0	0	0.407

Table 4: Lattice spacings for (Cr,Mo)N_x NaCl-type nitride (i) as calculated with a=4.15 Å (intermediate of the lattice parameter of CrN (4.14 Å, card 011-0065 in Ref. [22]), and that of γ-Mo_2N (4.163 Å, card 025-1366 in Ref. [22]) and (ii) as measured from the (average) diameters of the SADP ring patterns due to diffraction by the spherical particles in Fig. 11b. The relative intensity of the calculated reflections has been given in a qualitative manner in brackets in the first column. The d-spacing ranges of the rings given in the last column have been provided with a measurement error range assessed at 3 pixels of the detector.

reflection of (Cr,Mo)N_x	calculated d-spacing [Å] (a=4.15 Å)	observed d-spacing [Å]
1 1 1 (moderate)	2.396	2.45 (2.69-2.33)
2 0 0 (strong)	2.075	2.06 (2.17-2.01)
2 2 0 (strong)	1.467	1.46 (1.50-1.41)
3 1 1 (moderate) 2 2 2 (moderate)	1.251 1.198	1.23 (1.26-1.19)
4 0 0 (weak)	1.038	1.05 (1.07-1.02)
3 3 1 (weak) 4 2 0 (moderate/strong)	0.952 0.928	0.93 (0.95-0.91)